Comprehensive Summaries of Uppsala Dissertations
from the Faculty of Science and Technology 727

Anisotropy, disorder and frustration in magnetic nanoparticle systems and spin glasses

BY

PETRA JÖNSSON

ACTA UNIVERSITATIS UPSALIENSIS
UPPSALA 2002

Dissertation for the Degree of Doctor of Philosophy in Physics presented at Uppsala University in 2002

Abstract

Jönsson, P. 2002. Anisotropy, disorder and frustration in magnetic nanoparticle systems and spin glasses. Acta Universitatis Upsaliensis. *Comprehensive Summaries of Uppsala Dissertations from the Faculty of Science and Technology* 727. 71 pp. Uppsala. ISBN 91-554-5344-9.

Magnetic properties of nanoparticle systems and spin glasses have been investigated theoretically, and experimentally by squid magnetometry.

Two model three-dimensional spin glasses have been studied: a long-range Ag(11 at% Mn) Heisenberg spin glass and a short-range $Fe_{0.5}Mn_{0.5}TiO_3$ Ising spin glass. Experimental protocols revealing ageing, memory and rejuvenation phenomena are used. Quantitative analyses of the glassy dynamics within the droplet model give evidences of significantly different exponents describing the nonequilibrium dynamics of the two samples. In particular, non-accumulative ageing related to temperature-chaos is much stronger in Ag(11 at% Mn) than in $Fe_{0.5}Mn_{0.5}TiO_3$.

The physical properties of magnetic nanoparticles have been investigated with focus on the influence of dipolar interparticle interaction. For weakly coupled nanoparticles, thermodynamic perturbation theory is employed to derive analytical expressions for the linear equilibrium susceptibility, the zero-field specific heat and averages of the local dipolar fields. By introducing the averages of the dipolar fields in an expression for the relaxation rate of a single particle, a non trivial dependence of the superparamagnetic blocking on the damping coefficient is evidenced. This damping dependence is interpreted in terms of the nonaxially symmetric potential created by the transverse component of the dipolar field.

Strongly interacting nanoparticle systems are investigated experimentally in terms of spin-glass behaviour. Disorder and frustration arise in samples consisting of frozen ferrofluids from the randomness in particle position and anisotropy axes orientation. A strongly interacting system is shown to exhibit critical dynamics characteristic of a spin-glass phase transition. Ageing, memory and rejuvenation phenomena similar to those of conventional spin glasses are observed, albeit with weak temperature-chaos effects.

Petra Jönsson, Department of Materials Science, Uppsala University, Box 534, SE-751 21, Uppsala, Sweden. petra.jonsson@angstrom.uu.se

ISSN 1104-232X
ISBN 91-554-5344-9

Printed in Sweden by Eklundshofs Grafiska AB, Uppsala 2002

Till mina föräldrar

List of Publications

This thesis is based on the collection of articles given below.

I. **Nonequilibrium dynamics in a three-dimensional spin glass**
T. Jonsson, K. Jonasson, P. Jönsson, and P. Nordblad
Phys. Rev. B **59**, 8770 (1999).

II. **Memory and superposition in a spin glass**
R. Mathieu, P. Jönsson, D. N. H. Nam, and P. Nordblad
Phys. Rev. B **63**, 092401 (2001).

III. **Memory and chaos in an Ising spin glass**
R. Mathieu, P. E. Jönsson, P. Nordblad, H. Aruga Katori, and A. Ito
Phys. Rev. B **65**, 012411 (2002).

IV. **Domain growth and isothermal aging in 3d Ising and Heisenberg spin glasses**
P. E. Jönsson, H. Yoshino, P. Nordblad, H. Aruga Katori, and A. Ito
Submitted to Phys. Rev. Lett..

V. **Symmetrical Temperature-Chaos Effect with Positive and Negative Temperature Shifts in a Spin Glass**
P. E. Jönsson, H. Yoshino, and P. Nordblad
Submitted to Phys. Rev. Lett..

VI. **Nonlinear dynamic susceptibilities of interacting and noninteracting magnetic nanoparticles**
P. Jönsson, T. Jonsson, J. L. García-Palacios, and P. Svedlindh
J. Magn. Magn. Mater. **222**, 219 (2000).

VII. **Nonlinear susceptibility of superparamagnets with a general anisotropy energy**
J. L. García-Palacios, P. Jönsson, and P. Svedlindh
Phys. Rev. B **61**, 6726 (2000).

VIII. **Thermodynamic perturbation theory for dipolar superparamagnets**
P. E. Jönsson and J. L. García-Palacios
Phys. Rev. B **64**, 174416 (2001).

IX. Relaxation time of weakly interacting superparamagnets
P. E. Jönsson and J. L. García-Palacios
Europhys. Lett. **55**, 418 (2001).

X. Nonequilibrium dynamics in an interacting Fe-C nanoparticle system
P. Jönsson, M. F. Hansen, and P. Nordblad
Phys. Rev. B **61**, 1261 (2000).

XI. Spin glass like transition in a highly concentrated Fe-C nanoparticle system
P. Jönsson, P. Svedlindh, P. Nordblad, and M. F. Hansen
J. Magn. Magn. Mater. **226-230**, 1315 (2001).

XII. Critical dynamics of an interacting magnetic nanoparticle system
M. F. Hansen, P. E. Jönsson, P. Nordblad, and P. Svedlindh
J. Phys.: Condens. Matter *(accepted).*

XIII. Comment on "Erasing the glassy state in magnetic fine particles"
P. Jönsson and P. Nordblad
Phys. Rev. B **62**, 1466 (2000).

XIV. Fragility of the spin-glass-like collective state to a magnetic field in an interacting Fe-C nanoparticle system
P. E. Jönsson, S. Felton, P. Svedlindh, P. Nordblad, and M. F. Hansen
Phys. Rev. B **64**, 212402 (2001).

The author has also contributed to the following papers, not included in this thesis.

- **Adhesion-induced vesicle propulsion**
  I. Durand, P. Jönsson, C. Misbah, A. Valance, and K. Kassner
  Phys. Rev. E **56**, R3776 (1997)

- **The magnetic structure and properties of rhombohedral $Li_3Fe_2(PO_4)_3$**
  A. S. Andersson, B. Kalska, P. Jönsson, L. Häggström, P. Nordblad, R. Tellgren, and J. O. Thomas
  J. Mater. Chem. **10**, 2542 (2000)

- **Memory effects in an interacting magnetic nano-particle sample**
  P. Jönsson, M. F. Hansen, P. Svedlindh, and P. Nordblad
  Physica B **284-288**, 1754 (2000)

Contents

Chapter 1

Introduction

The research on spin glasses started in the 70's after the discovery of Cannella and Mydosh [1] of a peak in the ac susceptibility of diluted gold-iron alloys. Several different materials with various interaction mechanisms were soon found to exhibit this "new" magnetic behaviour, all with two properties in common – disorder and frustration. Spin glasses have since been widely studied, partly because they are excellent model systems of materials with quenched disorder. An understanding of spin glasses can thus contribute to the understanding of other, more complex and useful disordered systems, such as ceramic superconductors, polymers, gels and dense nanoparticle systems.

Magnetic nanoparticles are important examples of how a reduction in size changes the properties of a ferromagnetic material. For small enough particles it is energetically favourable to avoid domain walls and to form only one magnetic domain. The magnetism of such single-domain particles has been an active field of research since the pioneering work of Stoner and Wohlfarth [2] and Néel [3] in the late 40's. Due to new fabrication methods and characterisation techniques, the understanding and interest in nano-sized materials have increased explosively in the last years within the disciplines of physics, chemistry, material science and medicine. The development is also driven by a large number of applications: Nano-sized magnetic materials are used in, e.g. magnetic recording media, ferrofluids, catalysts and refrigerators. However, the interest in these systems is also of fundamental nature. Nanoparticles made up of a small number of spins can be used to study quantum tunnelling of magnetisation, and due to the interparticle dipolar interaction, which can be tuned by the particle concentration, nanoparticle systems may change their magnetic behaviour from superparamagnetic to spin-glass like.

The outline of this thesis is the following: In chapter 2 we survey some basic properties of classical spin systems and magnetism. Experimental protocols used in the study of disordered magnetism are also presented. Chapter 3 deals with spin glasses and nonequilibrium dynamics in the glassy phase. Two model spin glasses are compared, the long range Ag(11 at% Mn) Heisenberg spin glass and the short-range $Fe_{0.50}Mn_{0.50}TiO_3$ spin glass. In chapter 4 we discuss basic properties of non-interacting particle systems, and thermodynamic perturba-

tion theory is used to study weakly interacting particle systems. In chapter 5 we analyse the dynamics of a $Fe_{1-x}C_x$ nanoparticle system of different particle concentrations. The magnetic behaviour of the most concentrated samples is analysed in terms of spin-glass dynamics.

Chapter 2

Fundamentals

2.1 Spin systems

In order to explain magnetism one needs to use a quantum mechanical description. In this thesis we will study macroscopic manifestations of magnetism and only consider model spin-Hamiltonians. One such Hamiltonian, based on the quantum mechanical analysis of two hydrogen atoms, was proposed by Heisenberg in 1928 [4]:

$$\mathcal{H} = -\tfrac{1}{2}\sum_{i,j} J_{ij}\vec{s}_i \cdot \vec{s}_j - H\sum_{i=1}^{N} s_i^z \,, \tag{2.1}$$

where $\vec{s}_i$ is the spin which we will hereafter assume to be a classical unit vector, J_{ij} is the exchange coupling constant and the first summation is over nearest neighbours only. The N spins in the system are assumed to lie on a regular lattice. The second term in Eq. (2.1) is the Zeeman energy due to the coupling with the magnetic field H in the $\hat{z}$ direction. An even simpler model is due to Ising [5]. In this model the Hamiltonian is given by Eq. (2.1), but the spins only have discrete orientations $\vec{s}_i = s_i\hat{z}$, with $s_i = \pm 1$. The Ising system is a model system for strong uniaxial anisotropy.

If $J_{ij} = J > 0$, parallel orientation of the spins is favoured and at low temperatures all spins will be aligned ferromagnetically. For $J_{ij} = J < 0$, the low temperature phase is antiferromagnetic with the spins aligned antiparallel. If $J_{ij} = 0$ the Hamiltonian describes a system being paramagnetic at all temperatures.

In 1975 Edwards and Anderson (EA) [6] showed that the simple model spin Hamiltonian Eq. (2.1) with nearest-neighbour interaction could reproduce the cusp in the susceptibility versus temperature, which had been observed in experiments on spin glasses [1], provided that the coupling constants J_{ij} are chosen from a distribution fulfilling $\sum_{i,j} J_{ij} = 0$. For such symmetric spin glasses the two most common distributions are the Gaussian distribution

$$P(J_{ij}) = [2\pi J^2]^{-1/2}\exp[-J_{ij}^2/(2J^2)] \,, \tag{2.2}$$

with variance J^2 and the $\pm J$ distribution

$$P(J_{ij}) = \tfrac{1}{2}\delta(J_{ij} - J) + \tfrac{1}{2}\delta(J_{ij} + J)\,. \tag{2.3}$$

Sherrington and Kirkpatrick (SK) proposed in 1975 a model which is the infinite-range version of the EA-model [7]. It is assumed that any pair of spins interact with each other irrespective of their distance, with coupling constants chosen from a Gaussian distribution. To ensure a reasonable thermodynamic limit it is necessary that the variance scales with the number of spins in the system ($J^2 \propto N$).

In the EA-model not all the exchange interactions can be satisfied simultaneously, leading to *frustration* [8]. An example of frustration in the Ising $\pm J$ EA-model is given in Fig. 2.1. Here the frustration arises due to bond disorder, but it may also arise from randomness in spin positions (site disorder).

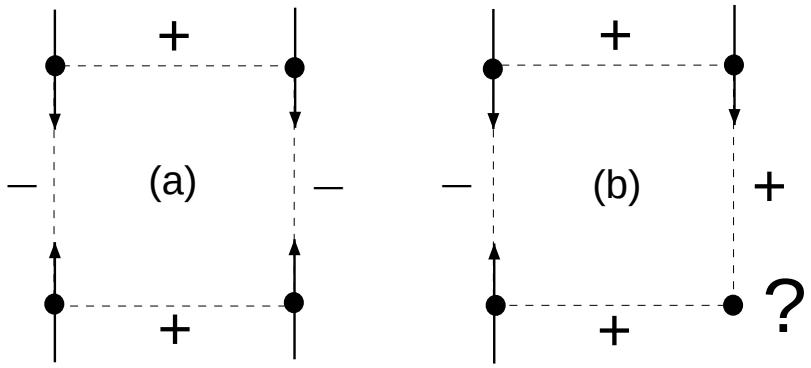

Figure 2.1: Examples of (a) an unfrustrated and (b) a frustrated spin configuration.

Magnetic nanoparticles, which will be discussed in chapter 4 and 5, have a macroscopic magnetic moment consisting of $10^2 - 10^5$ approximately parallel atomic spins acting coherently. In that context, we will describe the total magnetic moment as a classical spin (sometimes referred to as a *super spin*). The Hamiltonian of an ensemble of such spins can be given by Eq. (2.1) with an additional term due to magnetic anisotropy and J_{ij} determined by the dipolar interparticle interaction.

2.2 Thermodynamics

The *partition function* of a magnetic system is defined as

$$\mathcal{Z} = \sum_{\text{states}} \exp(-\beta\mathcal{H})\,,$$

where $\beta = 1/k_{\mathrm{B}}T$ and T is the temperature. In chapter 4 we will define the partition function for ensembles of magnetic nanoparticles and use it to calculate various thermodynamic quantities. The *free energy*, which for magnetic

systems is the Helmholtz free energy

$$\mathcal{F} = U - TS \tag{2.4}$$

where U is the internal energy and S is the entropy, can also be defined from the partition function

$$\mathcal{F}(T,H) = -k_{\mathrm{B}} T \ln \mathcal{Z}(T,H)\,. \tag{2.5}$$

All macroscopic thermodynamic properties can be obtained from differentiating the free energy (or equivalently the partition function). The internal energy and specific heat c_v are expressed in terms of the partition function as,

$$U = -\frac{\partial}{\partial\beta}(\ln \mathcal{Z})\,, \qquad \frac{c_v}{k_{\mathrm{B}}} = -\,\beta^2 \frac{\partial U}{\partial \beta}\bigg|_V = \beta^2 \frac{\partial^2}{\partial \beta^2}(\ln \mathcal{Z})\,. \tag{2.6}$$

The magnetisation in the direction of the applied field $M_z = \langle \vec{M} \cdot \hat{z} \rangle$ and the susceptibility χ are given by

$$M_z = -\frac{1}{\mu_0}\,\frac{\partial \mathcal{F}}{\partial H}\bigg|_T\,, \qquad \chi = \frac{1}{N}\,\frac{\partial M_z}{\partial H}\bigg|_T = -\frac{1}{\mu_0 N}\,\frac{\partial^2 \mathcal{F}}{\partial H^2}\bigg|_T\,. \tag{2.7}$$

Here $\langle \vec{M} \rangle$ stands for the statistical-mechanical average, i.e. the macroscopically accessible magnetisation in contrast to the magnetisation of a particular spin-state $\vec{M} = \sum \vec{s}_i$. The susceptibility can be related to the fluctuations in the magnetisation and equally to the spin-spin correlation function $\mathbf{\Gamma}_{ij}$

$$\chi = \frac{\mu_0 \beta}{N} \sum_{ij} \hat{z} \cdot \mathbf{\Gamma}_{ij} \cdot \hat{z}, \qquad \mathbf{\Gamma}_{ij} = \langle \vec{s}_i \vec{s}_j \rangle - \langle \vec{s}_i \rangle \langle \vec{s}_j \rangle\,. \tag{2.8}$$

The susceptibility obtained from the fluctuations corresponds to the *linear response*. The magnetic response to a small probing field ΔH, can be expanded as

$$\langle M_z \rangle - \langle M_z \rangle_{(\Delta H = 0)} = \chi \Delta H + \chi^{(2)} \Delta H^2 + \chi^{(3)} \Delta H^3 + \cdots\,, \tag{2.9}$$

where χ is the linear susceptibility and $\chi^{(n)}$ defines the nonlinear susceptibility of order n.

Although we have so far discussed only thermodynamic equilibrium properties, the spin-spin correlation function is in general a time dependent quantity, and hence, so are the susceptibility and the magnetisation.

2.3 Phase transitions

A phase transition is signalled by a singularity in the thermodynamic potential – which for magnetic systems is the free energy $\mathcal{F}$ defined by Eq. (2.4). If there is a finite discontinuity in the first derivative of the appropriate potential, the transition is of *first-order*. On the other hand, if the first derivative

is continuous, but second or higher-order derivatives are discontinuous or infinite, the transition is termed *continuous* (alternatively higher-order or critical). Most magnetic phase transitions are continuous and they are associated with an order parameter. The order parameter is zero in the disordered (paramagnetic) phase and becomes non-zero at the transition temperature T_c due to a spontaneous symmetry breaking. For a ferromagnet the order parameter is the magnetisation ($\sum_i s_i^z$), while for antiferromagnets it is the sublattice magnetisation. For spin glasses the magnetisation is zero at all temperatures and an appropriate order parameter was proposed by Edwards and Anderson [6] as the average value of the autocorrelation function

$$q_{\mathrm{EA}} = \lim_{t\to\infty} \langle \vec{s}_i(0) \cdot \vec{s}_i(t) \rangle \ . \tag{2.10}$$

Close to a continuous phase transition different thermodynamic quantities follow power laws of the reduced temperature ϵ, defined as

$$\epsilon = \frac{T - T_c}{T_c} \, , \tag{2.11}$$

with exponents called *critical exponents* (see some definitions in table 2.1). The critical exponents are related through scaling laws, see e.g Refs. [9, 10]. The critical exponents are important since they classify the phase transition; while T_c depends sensitively on the microscopic details of the system, the critical exponents are essentially universal, depending only on a few fundamental parameters. For models with short range interaction these parameters are the spatial dimension d and the symmetry of the order parameter. This concept of *universality classes* is one of the most important outcomes of the renormalisation group theory [11, 12]. The *lower critical dimension* defines the lowest dimension at which a system belonging to a certain universality class exhibits a phase transition at $T_c > 0$. For ferromagnets, Ising and Heisenberg systems belong to different universality classes; e.g. while the 2d Ising system exhibits a finite temperature phase transition, the Heisenberg system does not.

Table 2.1: Definition of some critical exponents

Zero-field specific heat	$C \sim \lvert\epsilon\rvert^{-\alpha}$
Order parameter	$q \sim (-\epsilon)^{\beta}$
Correlation length	$\xi \sim \lvert\epsilon\rvert^{-\nu}$
Order parameter susceptibility	$\chi \sim \lvert\epsilon\rvert^{-\gamma}$

2.4 Magnetic measurements

The aim of the experimental work in this thesis has been to study the time dependent magnetisation, $m(t)$, of spin glasses and magnetic nanoparticle systems. It has often been important to study $m(t)$ in a wide time window. The typical observation times for different measurement techniques are presented

in table 2.2. Measurements of both ac and dc magnetisation have been performed in a non-commercial low-field superconducting quantum interference device (squid) magnetometer [13]. The squid technique allows magnetisation measurements with high accuracy (10^{-8} emu).

Table 2.2: Characteristic observation times for various experimental techniques

Experimental technique	observation time
dc magnetisation	10^{-1} - 10^{6} s
ac magnetisation	10^{-6} - 10^{2} s
Mössbauer	10^{-9} - 10^{-7} s
Ferromagnetic resonance	10^{-9} s
Neutron scattering	10^{-12} - 10^{-8} s

From measurements of the magnetisation versus temperature, it is possible to determine if the system is in thermodynamic equilibrium or if irreversibility exists on the observed time-scale. In ac susceptibility measurements the magnetisation is probed by a small sinusoidal field of angular frequency ω. The dynamic susceptibility has one component in-phase (χ') and one out-of-phase (χ'') with the applied field. For dc magnetisation measurements, different (H,T)-protocols can be used to probe a magnetic system.

Zero-field-cooled (ZFC) magnetisation: the sample is cooled in zero magnetic field, a field is applied at the lowest temperature, and the magnetisation is recorded on reheating.

Field-cooled (FC) magnetisation: the sample is cooled in the measurement field, and the magnetisation is recorded either on cooling or heating.

Thermoremanent (TRM) magnetisation: the sample is cooled in a field and the magnetisation is recorded on reheating in zero field.

In thermodynamic equilibrium $\chi_{\mathrm{ZFC}} = \chi_{\mathrm{FC}} = \chi'$ while $\chi'' = \chi_{\mathrm{TRM}} = 0$. In an irreversible regime χ_{ZFC} is different from χ_{FC}, χ' is frequency dependent and both χ'' and χ_{TRM} are non-zero. For an example see Fig. 2.2.

We are however also interested in performing experiments that can disentangle nonequilibrium dynamics of disordered magnets from equilibrium dynamics of ergodic systems (e.g. independent nanoparticles). The nonequilibrium properties of glassy systems can be investigated by ZFC-relaxation experiments: The sample is quenched from a temperature in the paramagnetic state to a temperature in the nonstationary regime, and it is subsequently aged a wait time t_{w} before a probing field is applied and the magnetisation is measured as function of time. In a glassy system, the response of the system will depend on t_{w} - the system *ages*. No wait time dependence exists in an ergodic system. ZFC-relaxation curves for the canonical spin glass Ag(11 at %Mn) are shown in Fig. 2.3. It is convenient to plot the relaxation rate, $S(t) = 1/h\, dm(t)/d\ln t$, which more clearly reveals nonequilibrium effects. Ageing can also be observed

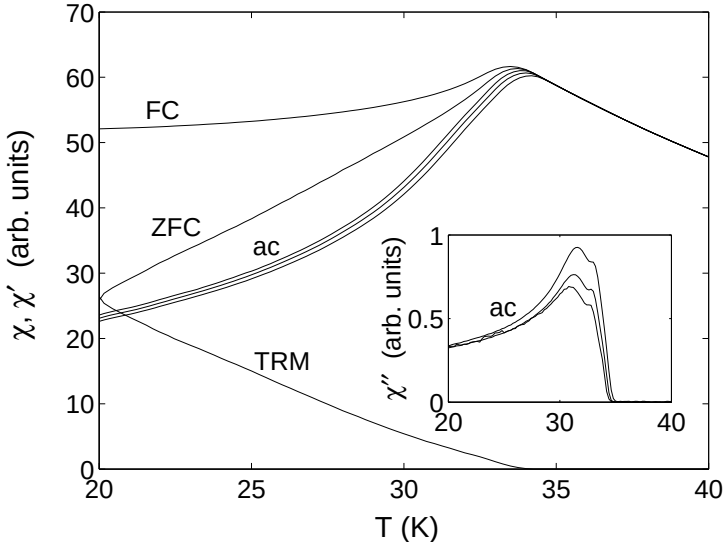

Figure 2.2: Dc and ac susceptibility for the canonical spin glass Ag(11 at% Mn). The inset shows the out-of-phase component of the ac susceptibility at frequencies $\omega/2\pi = 0.51$, 5.1, 55 Hz.

in the TRM-relaxation, as well as in isothermal ac susceptibility vs time experiments, where $\chi(t)$ relaxes only in a non-stationary regime. Additional information about the nonequilibrium properties can be obtained with more sophisticated (H,T,t)-protocols, which will be extensively discussed in this thesis.

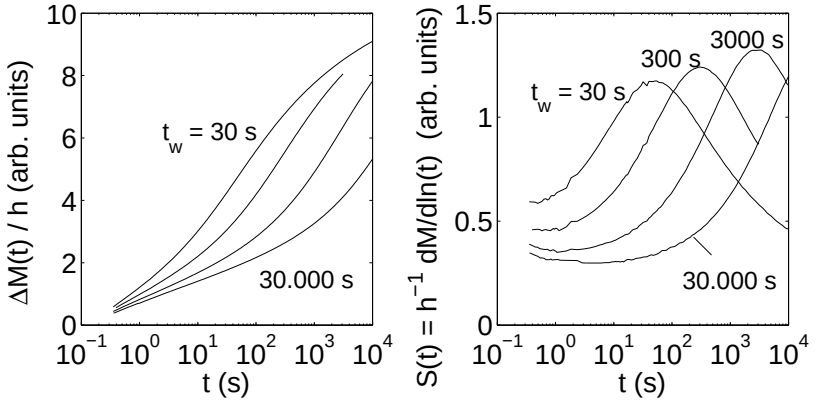

Figure 2.3: ZFC susceptibility (a) and relaxation rate (b) vs time on a logarithmic scale for the canonical spin glass Ag(11 at% Mn) at $T = 30$ K. The system has, prior to the field application, been aged for a time $t_{\rm w} = 30,\ 300,\ 3000,\ 30\,000$ s. The same arb. units as in Fig. 2.2.

Chapter 3

Spin glasses

3.1 Introduction

Since Cannella and Mydosh in 1972 discovered a peak in the ac susceptibility, and predicted the existence of a phase transition to a low temperature spin-glass phase, a large amount of work has been devoted to the existence of such a phase transition [14]. For 3d Ising spin glasses both experiments [15, 16, 17] and numerical simulations on the EA-model [18, 19, 20] clearly indicate the existence of a phase transition at a finite temperature $T_g \neq 0$. From experiments, it is clear that a finite temperature phase transition exists also for Heisenberg spin glasses [21, 22], while most numerical simulations indicate that $T_g = 0$ in 3d [23, 24, 25]. It has been proposed that the phase transition observed experimentally in Heisenberg systems is due to the chiral mechanism [24]; in the presence of weak random anisotropy the spins will couple to the chirality, inducing a phase transition at finite temperature, which belongs to a different universality class than the Ising spin glass [25, 26]. Also simulations on vector spin glasses with weak anisotropy support the existence of a phase transition at finite temperature [27, 28]. The critical exponents associated with the spin-glass phase transition derived from experiments are systematically scattered supporting the existence of different universality classes for spin glasses [29].

A question, still not solved, is how to adequately model the nonequilibrium dynamics in the spin-glass phase. The nonequilibrium properties are not unique for spin glasses [30, 31], but other materials have been shown to exhibit similar ageing, memory and rejuvenation phenomena. Examples of such materials are polymers [32], orientational glasses [33], gels [34], ceramic superconductors [35], and strongly interacting nanoparticle systems (see chapter 5). One important issue, now under hot debate, is the existence of temperature-chaos, predicted by the droplet model, and its relevance to the time scales of experiments and numerical simulations [36, 37, 38, 39, 40, 41].

In this chapter, we present specific experimental protocols that can be used to investigate the non-equilibrium dynamics of spin glasses and other glassy systems. We compare two model 3d spin glasses (one short-range Ising spin

glass and one long-range Heisenberg-like spin glass) concerning non-equilibrium dynamics. Particular interest is taken in the growth of the coherence length for equilibrium spin-glass order and non-accumulative effects revealing the existence of chaos with temperature. Quantitative investigations of model predictions are restricted to the droplet model.

3.2 Spin glass systems

The canonical spin-glass materials are noble metals (Au, Ag, Cu or Pt) weakly diluted with transition metal ions, such as Fe or Mn. The magnetic interaction in such systems is due to the scattering of the conduction electrons at the spins, leading to an indirect exchange interaction – the RKKY (Ruderman and Kittel [42], Kasuya [43] and Yosida [44]) interaction, which oscillates strongly with distance r between the spins:

$$J(r) = J_0 \frac{\cos(2k_{\mathrm{F}}r + \varphi_0)}{(k_{\mathrm{F}}r)^3} \,. \tag{3.1}$$

Here J_0 and φ_0 are constants and k_{F} is the Fermi wave vector of the host metal. Since the distances between the spins are random, some spin-spin interaction will be positive and favour parallel alignment while other will be negative thus favouring antiparallel alignment. This may result in a symmetric distribution $P(J) = P(-J)$ of bond strengths J.

The pure RKKY-interaction is isotropic and the canonical spin-glass systems are therefore often referred to as Heisenberg spin glasses. However, some anisotropy is present also in these systems originating from dipolar interaction and interaction of the Dzyaloshinsky-Moriya (DM) type [45]. The latter is due to spin-orbit scattering of the conduction electrons by non-magnetic impurities and reads,

$$E_{\mathrm{DM}} = -\vec{D}_{ij} \cdot (\vec{s}_i \times \vec{s}_j), \qquad \vec{D}_{ij} \propto \vec{r}_i \times \vec{r}_j \,, \tag{3.2}$$

where $\vec{D}_{ij}$ is a random vector due to the randomness of the spin positions $\vec{r}_i$. The dipolar interaction is, as will be discussed in Sec. 4.2.4, weak for spin systems, while the DM interaction is enhanced by the presence of non-magnetic transition-metal impurities [46, 45]. The Heisenberg system studied in this thesis is a polycrystalline sample of Ag(11 at% Mn) (**Ag**Mn).

A model system for a symmetric Ising spin glass is $Fe_xMn_{1-x}TiO_3$ with $x \approx 0.5$ [47, 48, 49]. Single crystals can be grown by the floating-zone method. Both $FeTiO_3$ and $MnTiO_3$ are antiferromagnets having easy-axis anisotropy along the hexagonal c-axis of the ilmenite structure (see Fig. 3.1). The Fe^{2+} spins in $FeTiO_3$ are coupled ferromagnetically within a c-layer and antiferromagnetically between adjacent c-layers. In $MnTiO_3$, on the other hand, both the intra-layer and inter-layer coupling of Mn^{2+} spins are antiferromagnetic. The compound $Fe_xMn_{1-x}TiO_3$ behaves as a spin glass for $0.4 \lesssim x \lesssim 0.57$, due to the mixing of ferromagnetic and antiferromagnetic interaction [49]. The perpendicular magnetisation is much smaller than the parallel magnetisation and does not show a cusp, which confirms the Ising-nature of this compound.

In $Fe_{0.5}Mn_{0.5}TiO_3$ the nearest-neighbour exchange interaction is the dominating interaction. The interaction is hence short-ranged in contrast to the long-ranged RKKY-interaction in canonical spin glasses.

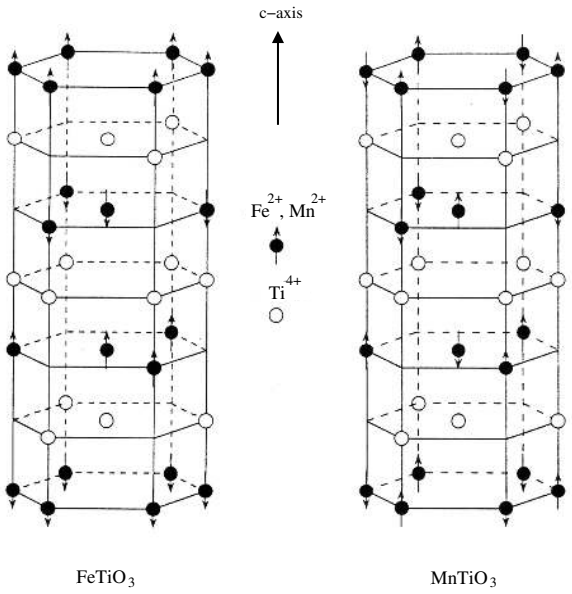

Figure 3.1: Hexagonal structure of the ilmenite-type compounds $FeTiO_3$ and $MnTiO_3$. The O^{-2} ions are omitted. From Ref. [50].

3.3 Spin glass theory

The basis for most numerical and analytical modelling of spin glasses is the spin Hamiltonian presented in Sec. 2.1 with either short-range interaction (the EA-model) or infinite-range interaction (the SK-model).

There are two main theories: the "droplet" theory [51, 52, 53, 54, 55] based on renormalisation group arguments for the Ising EA-model, and the replica symmetry breaking theory of Parisi [56, 57, 58] providing a mean-field solution to the SK-model. We will here restrict our interpretations of experimental observations to real-space models (the original droplet model and some extensions [59, 38]). One basic property of a real-space model is to provide a means for converting the experimentally accessible parameters temperature and time into the coherence length for equilibrium spin-glass order. A knowledge of the domain growth law will allow further quantitative investigations of various properties of the spin-glass phase.

3.3.1 Critical dynamics

Close to the transition temperature T_g, the dynamics of a spin-glass system will be governed by critical fluctuations, but critical fluctuations are also of

importance on experimental time scales quite far from T_g. At temperatures both below and above T_g, length scales shorter than the coherence length of the critical fluctuations

$$\xi \sim L_0|\epsilon|^{-\nu}\,, \tag{3.3}$$

will be dominated by critical fluctuations. Here L_0 is a microscopic length scale and the reduced temperature ϵ is defined in Eq. (2.11). The coherence length can be transformed into a time scale according to conventional critical slowing down; the critical correlation time is given by

$$\tau_c \sim \tau_m(\xi(T)/L_0)^z \sim \tau_m|\epsilon|^{-z\nu}\,, \tag{3.4}$$

with τ_m being a microscopic time scale. For $T > T_g$, the system is in equilibrium on length (time) scales longer than ξ (τ_c) and hence the magnetic response is paramagnetic. At temperatures below T_g, there is a crossover between critical dynamics on short length (time) scales and activated dynamics on long length (time) scales. The length scale of critical dynamics as a function of temperature is illustrated in Fig. 3.2. Activated dynamics and the crossover from critical dynamics will be discussed in detail below.

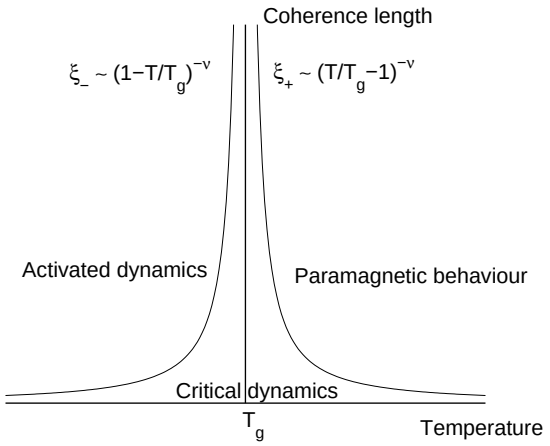

Figure 3.2: Illustration of length (time) scales in spin glasses.

3.3.2 The droplet model

The starting point of the droplet model is the Ising EA-model with a continuous distribution of independent exchange. Temperatures in the spin glass phase not too close to T_g are considered. At each temperature the equilibrium state is considered to consist of a ground state plus thermally activated droplet excitations of various size. It is assumed that there exists exactly one ground state (and its global spin reversal). A droplet is a low-energy compact cluster of spins with a volume L^d and a fractal surface area L^{d_s}. The fractal exponent d_s fulfils $d-1 < d_s < d$ and has been estimated to $d_s \approx 2.58$ in 3d [60].

The typical droplet free energy scale as

$$F_L^{\rm typ} \sim \Upsilon(T)(L/L_0)^\theta\,, \qquad \Upsilon(T) \sim J\epsilon^{\theta\nu}\,, \tag{3.5}$$

where θ is the stiffness exponent and $\Upsilon(T) \sim J\epsilon^{\theta\nu}$ is the stiffness. Fisher and Huse argued that $\theta < (d-1)/2$ [54]. The droplet free energy is broadly distributed, and due to the presence of configurations which are almost degenerate with the ground state, the distribution of F_L will have weight down to zero energy,

$$\rho_L(F_L) \approx \tilde{\rho}(F_L/F_L^{\rm typ})/F_L^{\rm typ}, \qquad \tilde{\rho}(0) > 0. \tag{3.6}$$

If $\theta < 0$ large droplets can be flipped at a low energy cost so that the large droplets will not be stable against small fluctuations and the system will be paramagnetic. Hence, a negative value of θ indicates that the system is below its lower critical dimension d_l [61, 51]. On the other hand, if $\theta > 0$ very few of the large scale droplets will be thermally activated since $F_L^{\rm typ} > k_{\rm B}T$. Since $\rho_L(F_L)$ has non-zero weight near zero a certain fraction of droplets will be thermally active and dominate most of the equilibrium physics. For Ising spin glasses $\theta \approx -0.3$ in 2d [62, 63] and $\theta \approx 0.2$ in 3d [61, 64, 65], which tells us that $2 < d_l < 3$ for Ising spin glasses within the droplet model.

The dynamics of droplets is considered to be a thermally activated process. The energy barrier for annihilation of a droplet will scale as

$$B_L^{\rm typ} \sim \Delta(T)(L/L_0)^\psi\,, \qquad \Delta(T) \sim J\epsilon^{\psi\nu}\,, \tag{3.7}$$

where $\Delta(T)$ sets the free-energy scale of the barriers and ψ is an exponent satisfying $\theta < \psi < d-1$. The characteristic time τ_L that a thermally activated droplet will last for is given by an Arrhenius law

$$\ln[\tau_L/\tau_0(T)] \sim B_L/k_{\rm B}T\,, \tag{3.8}$$

where $\tau_0(T)$ is the unit time scale for the activated process. For activated hopping processes the unit time scale is *not* simply given by the real microscopic time scale [66], which is $\tau_m \sim \hbar/J \sim 10^{-13}$ s in spin systems. A plausible choice for $\tau_0(T)$ is instead the critical correlation time τ_c as proposed in Ref. [55].

The Arrhenius law implies that droplets of length scale $L = L_T(t)$,

$$L_T(t) \sim \left[\frac{k_{\rm B}T\ln(t/\tau_0(T))}{\Delta(T)}\right]^{1/\psi}\,, \tag{3.9}$$

can be activated within a time scale t. Hence $L_T(t)$ will be the characteristic length scale of equilibrium spin-glass order at a time t after a quench from a temperature above $T_{\rm g}$ to a temperature T in the spin-glass phase. In a magnetisation measurement the system is probed by applying a small magnetic field. The magnetisation arises through the polarisation of droplets. Since this polarisation also is a thermally activated process, it will affect droplets of size $L(t_{\rm obs})$, where $t_{\rm obs} = 1/\omega$ (in an ac experiment at a given angular frequency ω) or the time elapsed after the application of the magnetic field in a ZFC-relaxation experiment.

Isothermal ageing

In the droplet model it is assumed that isothermal ageing at a constant temperature T after a quench from a temperature above the spin-glass transition temperature $T_{\rm g}$ is a coarsening process of domain walls as in many other phase ordering systems. During the isothermal ageing of a spin glass of spatial dimension d, the temporal ac susceptibility at a given angular frequency ω at time t after the quench is supposed to scale as [55, 67],

$$\frac{\chi''(\omega,t)-\chi''_{\rm eq}(\omega)}{\chi''(\omega,t)} \propto \left[\frac{L_T(1/\omega)}{L_T(t)}\right]^{d-\theta} , \tag{3.10}$$

where $L_T(t)$ is the typical size of the domains and $L_T(1/\omega)$ is the largest size of the droplets being polarised by the ac field. The left hand side of this equation can equally well be written $[\chi''(\omega,t)-\chi''_{\rm eq}(\omega)]/\chi''_{\rm eq}(\omega)$. Both scaling forms are expected to give the same result, if correction terms of order $[L_T(1/\omega)/L_T(t)]^{2(d-\theta)}$ are negligible. The basic physical idea of this scaling form is that the presence of a domain wall effectively reduces the excitation free energy of droplet excitations that are touching the domain wall. This reduction can be accounted for by defining an effective stiffness $\Upsilon_{\rm eff}$, which for small values of $L_T(1/\omega)/L_T(t)$ will scale as $1-\Upsilon_{\rm eff}/\Upsilon \propto [L_T(1/\omega)/L_T(t)]^{d-\theta}$ [55].

The equilibrium ac susceptibility $\chi''_{\rm eq}(\omega)$ is proposed to scale as [54],

$$\chi''_{\rm eq}(\omega) \approx \frac{\pi}{2} K_\omega \frac{q_m(T)}{\Upsilon(T)} \frac{\partial}{\partial \ln \omega} \left[\frac{L_0}{L_T(1/\omega)}\right]^{\theta} , \tag{3.11}$$

where K_ω is a universal constant and q_m is equal to the Edwards-Anderson order parameter for a symmetric spin glass.

Cross-over between critical dynamics and activated dynamics

Due to a possible slow crossover from critical dynamics at $t \ll \tau_c(T)$ to activated dynamics at $t \gg \tau_c(T)$, the logarithmic domain growth law Eq. (3.9) may apply only for ideally asymptotic regimes beyond the time scales of numerical simulations [68, 59, 39]. Results from numerical simulations [69, 70, 71] accordingly suggest an alternative growth law for the spin glass coherence length

$$L_T(t) \sim L_0 (t/\tau_m)^{1/z(T)} , \tag{3.12}$$

where $z(T) \simeq z(T_{\rm g}/T)$ is a temperature-dependent effective exponent.

Bouchaud et al. [38] proposed to relate time and length according to

$$t \sim \tau_0 (L_T(t)/L_0)^z \exp\left[\frac{\Delta(T)(L_T(t)/L_0)^\psi}{k_{\rm B}T}\right] . \tag{3.13}$$

This formula is asymptotically correct both in the limit of critical and activated dynamics.

Temperature chaos

According to the droplet theory, typical spin configurations of a pair of equilibrium states at two different temperatures, say T_1 and T_2, are essentially the same on short length scales much below the so-called overlap length $L_{\Delta\mathrm{T}}$, but completely different on large length scales much beyond $L_{\Delta\mathrm{T}}$. This temperature-chaos is due to a subtle competition between energy and entropy in the spin-glass phase.

In the limit of small temperature differences $|\Delta T/J| \ll 1$, the overlap length between the two temperatures T_1 and $T_2 = T_1 + \Delta T$ is supposed to scale as [72, 54, 55]

$$L_{\Delta\mathrm{T}} \sim L_0 |\Delta T/J|^{-\zeta}\,, \qquad \zeta = 2/(d_\mathrm{s} - 2\theta)\,, \tag{3.14}$$

where ζ is the chaos exponent.

3.3.3 Spin glass order in a magnetic field?

Within the droplet model, a spin glass is disordered by an applied magnetic field H on length scales larger than the correlation length [54]

$$\xi_H \propto \left[\frac{\Upsilon}{H\sqrt{q_m}}\right]^{2/(d-2\theta)}\,, \tag{3.15}$$

while it still exhibits spin-glass order on shorter length scales. The droplet model therefore predicts that a spin glass will not exhibit a phase transition in a magnetic field. This prediction has been experimentally confirmed for the $Fe_{0.50}Mn_{0.50}TiO_3$ sample [73].

In the mean field model, the spin glass order will persist up to the the d'Almeida-Thouless line [74] for Ising spin glasses (or weak fields) or the Gabay-Toulouse line [75] for Heisenberg spin glasses in strong fields. Recently, Kawamura and Imagawa [76] showed that the chiral-glass ordered state sustains in a magnetic field in a similar way as predicted by the mean-field model. This is supported by experiments on Heisenberg spin glasses [77].

3.4 Experiments: Ageing, memory and rejuvenation

Magnetic ageing was first observed by Lundgren et al. in 1983 [78]. It was found that the ZFC-relaxation depends on the wait time, t_w, the system has been allowed to age at the measurement temperature, before the probing field is applied and the magnetisation is recorded as a function of time (t_obs), see Fig. 2.3. The peak observed in the relaxation rate at $t_\mathrm{obs} \approx t_\mathrm{w}$ has, within the droplet model, been interpreted as a crossover between quasi-equilibrium dynamics at $L(t_\mathrm{obs}) < L(t_\mathrm{w})$ and nonequilibrium dynamics at $L(t_\mathrm{obs}) > L(t_\mathrm{w})$ (see [59] for more details). Later, experimental protocols including temperature steps and cyclings were proposed [79]. These experiments showed that

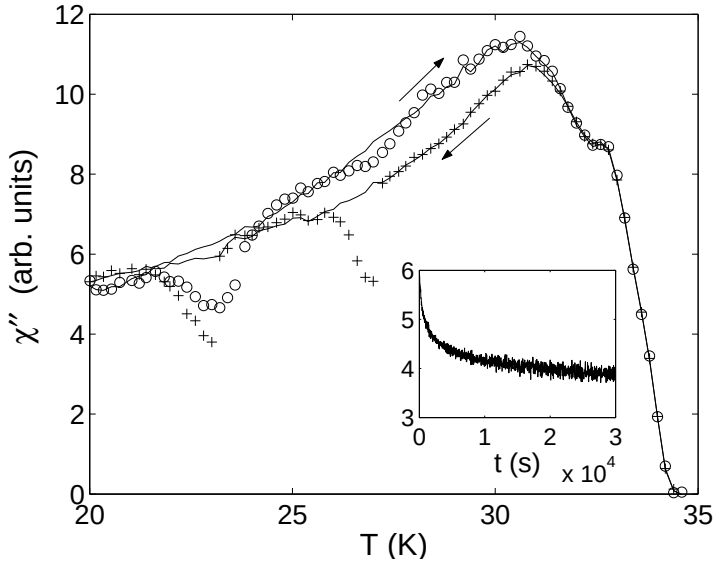

Figure 3.3: $\chi''(\omega)$ vs temperature for the **Ag**Mn sample measured during cooling (pluses) and during the subsequent re-heating (circles). Two intermittent halts were made during the cooling: One at 27 K for 10 000 s and another at 23 K for 30 000 s. The susceptibility measured on constant cooling and on constant heating is shown as reference (solid lines). The inset shows $\chi''(\omega)$ vs time during the halt at $T = 23$ K; $\omega/2\pi = 510$ mHz.

spin-glass order, characteristic of different temperatures, can co-exist on different length scales, and the findings could qualitatively be interpreted within the droplet model supporting the temperature-chaos scenario [80]. Recently, a simple experimental protocol was employed to illustrate memory and rejuvenation effects [36]; the sample is cooled from a high temperature with one (or more) halts at a low temperature in the spin-glass phase during the cooling. The ac susceptibility is subsequently recorded on heating. Such a "memory" experiment is shown in Fig. 3.3. The ac susceptibility is measured on cooling with two intermittent stops. During the isothermal ageing the ac susceptibility relaxes as shown in the inset of the figure. As the cooling is resumed the ac susceptibility merges with the reference curve - the system is *rejuvenated*. On the subsequent reheating the ac susceptibility shows a dip around each of the ageing temperatures - the system has kept a *memory* of each isothermal ageing.

In Ref. [36] it was argued that this "double memory" experiment is incompatible with the compact domain growth picture of the droplet model. In Paper I, it was instead proposed that the domains are fractal (fractal domains have also been proposed in Ref. [81, 82, 83]). While Yoshino et al. [37] used numerical simulations, putting chaos in by hand, to show that the memory effect is dynamic in nature, and due to the existence of "ghost domains" it does not contradict the standard droplet picture. These ghost domains are the equilibrium domains grown during the first ageing at the higher temperature,

which will only partly be erased during the ageing at the lower temperature, due to the large separation in length scales at the same time scales for different temperatures. This leads us to the importance of knowing the growth law for the coherence length when comparing experiments with real space models. In an experiment, we can control the two parameters temperature and time, but for interpretations we are interested in the length scale of equilibrium domains.

We have performed experiments on the two model spin glasses $Fe_{0.5}Mn_{0.5}TiO_3$ and **Ag**Mn. When comparing these experimental findings with theoretical models concerning nonequilibrium dynamics, it is important to take into account that what we refer to as a "quench" is not an ideal quench but a rapid cooling, with a finite cooling rate ($\sim 0.05 - 0.08$ K/s in our magnetometer). The system will therefore have an "effective age" when reaching the measurement temperature. This age is 10-30 s for the **Ag**Mn sample and $100 - 350$ s for the $Fe_{0.50}Mn_{0.50}TiO_3$ sample depending on the measurement temperature. The difference in effective age between the two samples is due to a difference in their chaotic nature as will be discussed below.

3.4.1 Isothermal ageing

By scaling isothermal ageing data to the predictions of the droplet model [Eq. (3.10)], it is possible to test the functional form of the domain growth law and estimate exponents. In earlier studies [84, 65, 31] an ωt-scaling, indicating an algebraic growth law [c.f. Eq. (3.12)], has been found. It was also found that the data could not be described by a $\ln t/\ln\omega$ behaviour consistent with a logarithmic domain growth law. However in those investigations it was assumed that $\tau_0(T) = \tau_m$. The effect of isothermal ageing was measured by recording the ac susceptibility, as a function of time, after rapidly cooling the spin glasses from a temperature above T_g to the measurement temperature (the relaxation of the ac susceptibility as a function of time at a constant temperature is shown in the inset of Fig. 3.3).

The isothermal ageing data were analysed using the scaling prediction from the droplet model Eq. (3.10) and the logarithmic domain growth law in Eq. (3.9), yielding

$$\frac{\chi''(\omega,t) - \chi''_{\rm eq}(\omega)}{\chi''(\omega,t)} \propto \left\{ \frac{\ln[t/\tau_c(T)]}{\ln[(1/\omega)/\tau_c(T)]} \right\}^{\frac{d-\theta}{\psi}} . \tag{3.16}$$

This scaling law should permit all isothermal ageing data from measurements at different temperatures and frequencies to collapse onto one *single* master curve. A necessary condition for such a scaling is activated dynamics, i.e. $t > (1/\omega) \gg \tau_c(T)$. Provided that the critical correlation time was chosen as the unit time scale ($\tau_0(T) = \tau_c$), it was possible to scale the data for both samples (see Fig. 3.4), while it was not possible to scale the data for any of the two spin glasses using a constant value for $\tau_0 \sim 10^{-13}$ s.

The remaining parameter in the scaling analysis, $\chi''_{\rm eq}(\omega,T)$, is predicted to show a frequency and temperature dependence according to Eq. (3.11), i.e. $\chi''_{\rm eq}(\omega) \propto [T\ln((1/\omega)/\tau_c(T))]^{-(1+\theta/\psi)}$. We have from these analyses obtained

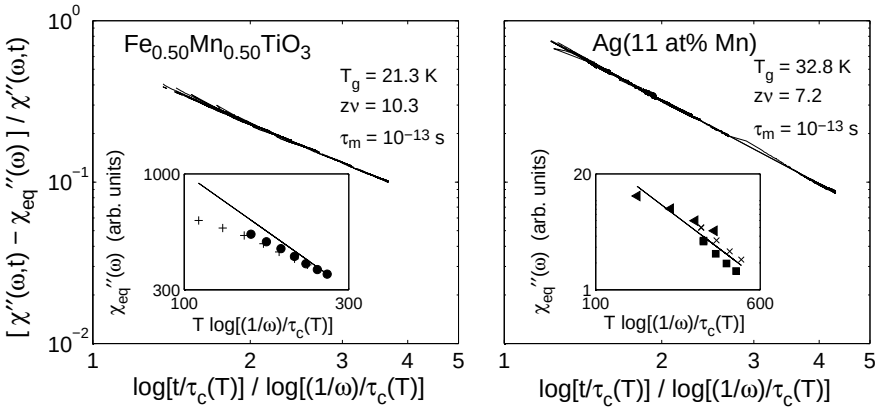

Figure 3.4: $[\chi''(\omega,t) - \chi''_{\rm eq}(\omega)]/\chi''(\omega,t)$ vs $\ln[t/\tau_c(T)]/\ln[(1/\omega)/\tau_c(T)]$ on a log-log scale (a) for the $Fe_{0.50}Mn_{0.50}TiO_3$ sample with $\omega/2\pi = 0.17, 0.51, 1.7, 5.1, 17, 55, 170$ Hz, $T = 15, 17$ K and (b) for the **Ag**Mn sample with $\omega/2\pi = 0.17, 1.7, 17, 170$ Hz, $T = 20, 25, 30$ K. The insets show $\chi''_{\rm eq}(\omega)$ vs $\ln[(1/\omega)/\tau_c(T)]$ on a log-log scale at (a) $T = 17$ K (pluses) and 15 K (circles), and (b) $T = 30$ K (triangles), 25 K (crosses) and 20 K (squares).

estimates of θ and ψ (see Paper IV) and the results are summarised in table 3.1 together with earlier estimates.

The difference in the estimated exponents between the scaling form with $\chi''(\omega,t)$ in the denominator and that with $\chi''_{\rm eq}(\omega)$, tells us that correction terms of order $[L_T(1/\omega)/L_T(t)]^{2(d-\theta)}$ are not negligible. However, the difference can give an indication of the error in the values. Also, the slow crossover from critical to activated dynamics may require a more complete functional form than only the asymptotic form Eq. (3.9) to accurately describe the growth law on experimental time scales.

The significant difference between the exponents obtained for the $Fe_{0.50}Mn_{0.50}TiO_3$ Ising spin glass and the **Ag**Mn Heisenberg spin glass is consistent with the chiral-glass picture conjecturing a different universality class for Heisenberg spin glasses than for Ising spin glasses. Experimental evidences for

Table 3.1: Droplet exponents

	$Fe_{0.50}Mn_{0.50}TiO_3$		**Ag**Mn	
From	θ	ψ	θ	ψ
$[\chi''(\omega,t) - \chi''_{\rm eq}(\omega)]/\chi''(\omega)$	0.2	1.9	1.0	1.2
$[\chi''(\omega,t) - \chi''_{\rm eq}(\omega)]/\chi''_{\rm eq}(\omega)$	0.13	1.3	0.6	0.8
Exp. [73]	-	0.8	-	-
Exp. [85, 38]	-	0.3-0.7	-	1.3

	Ising		Heisenberg	
Ising EA-model [61, 64, 65]	0.2	-	-	-
Heisenberg EA-model [86]	-	-	0.8	-

different universality classes were recently obtained by magnetic torque measurements [29].

3.4.2 Memory, ageing and rejuvenation

The cooling/heating rate dependence of the susceptibility of a **Ag**Mn spin glass was investigated in Paper I. The slower the cooling rate the lower is the susceptibility curve and hence, the system is "older" or closer to equilibrium. As noticed in the isothermal ageing study it is not possible to reach a truely stationary regime on experimental time scales even for quite high frequency ac susceptibility measurements. For the **Ag**Mn sample, the ac susceptibility curve measured on cooling is lower than the curve subsequently measured on heating except close to the lowest temperature (see Fig. 3.3). If the ageings at different temperatures were accumulative, the heating curve would appear older than the cooling curve and therefore lower. For the $Fe_{0.50}Mn_{0.50}TiO_3$ sample this is indeed the case (see Fig. 3.5). The non-accumulative behaviour observed in the cooling-heating curves of the ac susceptibility of the **Ag**Mn sample can qualitatively be explained by rejuvenation during cooling and heating due to strong temperature chaos. For the $Fe_{0.50}Mn_{0.50}TiO_3$ sample the double memory experiment shown in Fig. 3.5 indicates that temperature-chaos does exist, but that it is much weaker than for **Ag**Mn .

A dc method to investigate effects of memory and rejuvenation was employed in Papers II and III. The ZFC, FC and TRM magnetisations are mea-

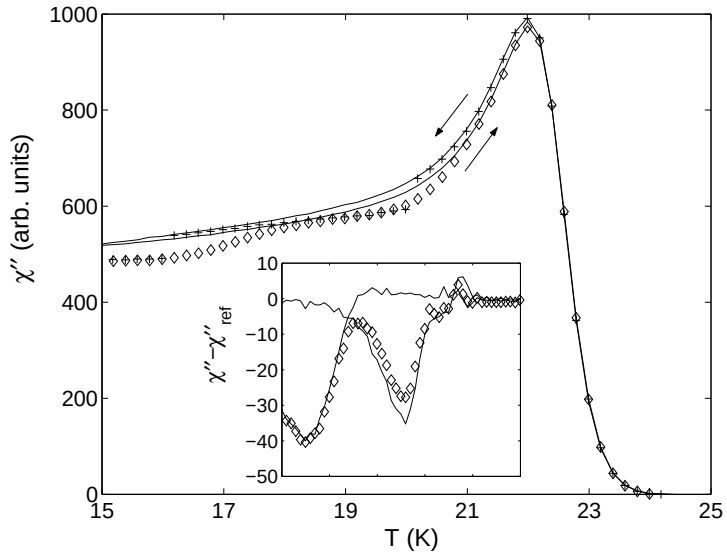

Figure 3.5: a) χ'' vs temperature measured on cooling (pluses), with two intermittent stops at 20 K for 10 000 s and at 16 K for 30 000 s, and on the subsequent reheating (diamonds), for the $Fe_{0.50}Mn_{0.50}TiO_3$ sample. The reference cooling and heating curves are drawn with solid lines. Inset: $\chi'' - \chi''_{\rm ref}$ vs temperature derived from the heating curves for single and double stops. $\omega/2\pi = 510$ mHz.

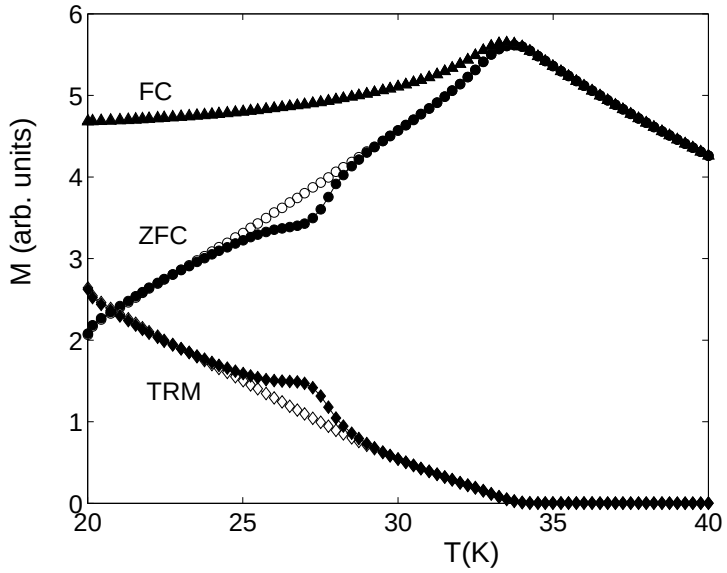

Figure 3.6: ZFC, FC and TRM magnetisation vs temperature for the **Ag**Mn sample. Filled symbols denotes measurements with a stop at $T = 27$ K for 10^4 s and open symbols the reference measurements.

sured as described in section 2.4, but with one (or more) stop(s) during the cooling. The stop during the cooling results in a "dip" in the ZFC magnetisation, an "excess" in the TRM magnetisation while the FC magnetisation is only marginally affected, see Fig. 3.6. The advantage of this dc-memory method, compared to the ac memory method, is that the measurements are easier to perform, but still yield information about memory, chaos and rejuvenation.

Chaos and overlap

From the experiments presented above one can in a simple way get an idea about chaos and rejuvenation in the spin-glass phase. In order to make quantitative studies, T-shift experiments have been performed using the following protocol: the system is quenched from a temperature above the spin-glass transition temperature $T_{\rm g}$ to an initial temperature $T_i < T_{\rm g}$, at which it is aged a time $t_{\rm w}$. The temperature is then shifted to a measurement temperature $T_m = T_i - \Delta T$ with ΔT being either positive or negative. Immediately after reaching temperature stability at T_m either the ZFC magnetisation or the ac susceptibility is recorded as a function of time. This T-shift experiment is denoted as (T_i, T_m).

In Paper V we extract the effective age $t_{\rm eff}$ of the system at T_m due to the ageing at T_i from the maximum in the relaxation rate $S(t)$. The relaxation rate is shown in Fig. 3.7 for different values of ΔT for the **Ag**Mn sample. We have also measured the ac relaxation and used the method of Refs. [65, 85, 39] to determine $t_{\rm eff}$. The extracted value of $t_{\rm eff}$ did not depend on how the system was

probed, which validates both methods. However, we found the determination of $t_{\rm eff}$ somewhat more ambiguous in the ac case.

If temperature-chaos is absent, successive ageing at the two different temperatures will add to each other in a fully accumulative way. In such a situation the effective age $t_{\rm eff}$ is a monotonically increasing function of $t_{\rm w}$, $t_{\rm eff} = f(t_{\rm w}, (T_i, T_m))$ and conversely $t_{\rm w} = f^{-1}(t_{\rm eff}, (T_i, T_m))$. By performing twin-experiments – (T_1, T_2) and its conjugate (T_2, T_1) – for pairs of temperatures T_1 and T_2 below T_g, it can be checked if the *criterion for accumulative ageing*

$$f^{-1}\left(t, (T_1, T_2)\right) = f\left(t, (T_2, T_1)\right) \tag{3.17}$$

holds.

Data from twin-experiments on the **Ag**Mn sample are shown in Fig. 3.8 and on the $Fe_{0.50}Mn_{0.50}TiO_3$ sample in Fig. 3.9. The results of (T_1, T_2) experiments are shown with $t_{\rm w}$ on the horizontal axis and $t_{\rm eff}$ on the vertical axis. The results of (T_2, T_1) experiments are shown in the reversed way - with $t_{\rm eff}$ on the horizontal axis and $t_{\rm w}$ on the vertical axis. The criterion for accumulative ageing [Eq. (3.17)] is satisfied if and only if the two data sets merge with each other in the plots. Clear non-accumulative effects are observed for $\Delta T \gtrsim 0.2$ K ($\Delta T/T_g \gtrsim 0.006$) for the **Ag**Mn sample and for $\Delta T > 1$ K ($\Delta T/T_g > 0.05$) for the $Fe_{0.50}Mn_{0.50}TiO_3$ sample. This confirms the existence of temperature-chaos and that the spin-glass phase in the **Ag**Mn sample is more chaotic than the spin-glass phase in the $Fe_{0.50}Mn_{0.50}TiO_3$ sample.

A quantitative analysis of the non-accumulative effect in terms of the droplet theory was done in Paper V for the **Ag**Mn sample. The effective coherence

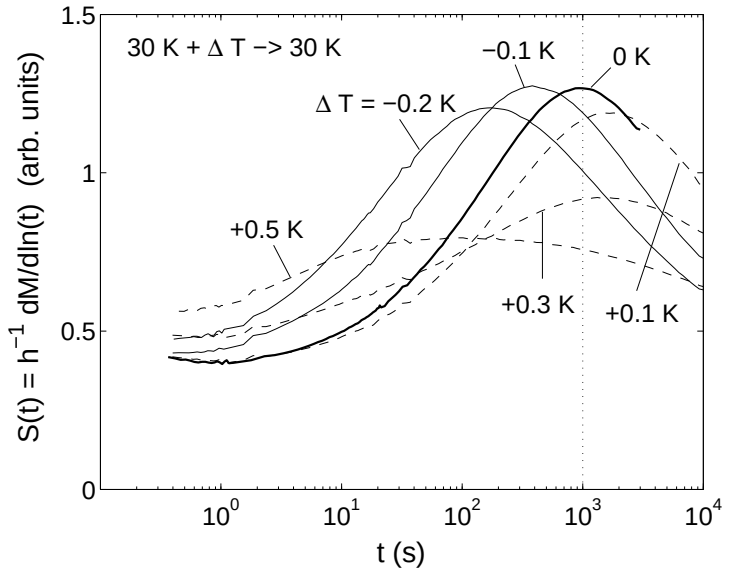

Figure 3.7: Relaxation rate vs time on a logarithmic scale for the **Ag**Mn sample measured at $T_m = 30$ K after ageing at $T_m + \Delta T$ for $t_{\rm w} = 1000$ s.

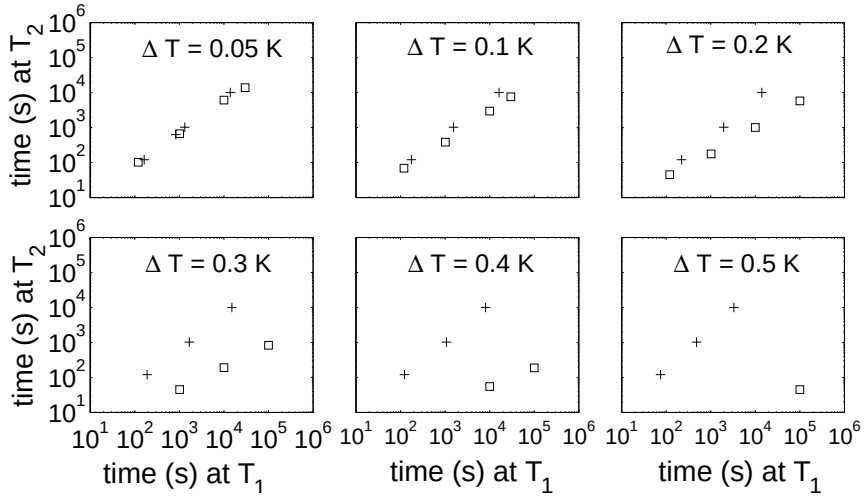

Figure 3.8: Relation between $t_{\rm w}$ and $t_{\rm eff}$ in twin-experiments – (T_1, T_2) shown as squares and (T_2, T_1) shown as pluses – on the **Ag**Mn sample. $T_1 = (30 - \Delta T)$ K and $T_2 = 30$ K with ΔT=0.05, 0.1, 0.2, 0.3, 0.4 and 0.5 K.

length $L_{\rm eff}$ at T_m, due to the ageing at T_i was determined as

$$L_{\rm eff} = L_{T_m}(t_{\rm eff}), \tag{3.18}$$

using the growth law Eq. (3.9) with the parameters obtained by the isothermal ageing analysis together with $\nu = 1.1$ and $J = T_{\rm g}$. For the data with accumulative ageing $L_{\rm eff} = L_{T_i}(t_{\rm w})$, which satisfies Eq. (3.17), and for data with non-accumulative ageing; the data of the (T_1, T_2) and (T_2, T_1) experiments merge with each other. The latter clearly demonstrates that the effective domain size for a given pair of temperatures is the same, which is consistent with the expectation that there is a unique overlap length between a given pair of temperatures.

Fully accumulative ageing, i.e. $L_{\rm eff} = L_{T_i}(t_{\rm w})$, will only be observed on length scales $L_{T_i}(t_{\rm w}) \ll L_{\Delta \rm T}$, where $L_{\Delta \rm T}$ is the overlap length. $L_{\rm eff}$ saturates to $L_{\Delta \rm T}$ on length scales $L_{T_i}(t_{\rm w}) \gg L_{\Delta \rm T}$. A simple possibility is then that the two limits are connected by a crossover scaling form,

$$\frac{L_{\rm eff}}{L_{\Delta \rm T}} = F\left(\frac{L_{T_i}(t_{\rm w})}{L_{\Delta \rm T}}\right), \tag{3.19}$$

with a scaling function $F(x) = x$ for $x \ll 1$ (accumulative ageing) and $F(x) = 1$ for $x \gg 1$ (chaos). Note that the intermediate regime between the two extremes can be a very slow crossover.

Figure 3.10 shows a scaling plot, for the **Ag**Mn sample, to fully test Eq. (3.19) using a large set of data for a variety of ΔT's. A good collapse of the data is obtained for $\zeta = 2.6 \pm 0.5$. Since the time (length) scales we can study are restricted, we did not reach the chaotic limit where $L_{\rm eff}$ is determined by $L_{\Delta \rm T}$.

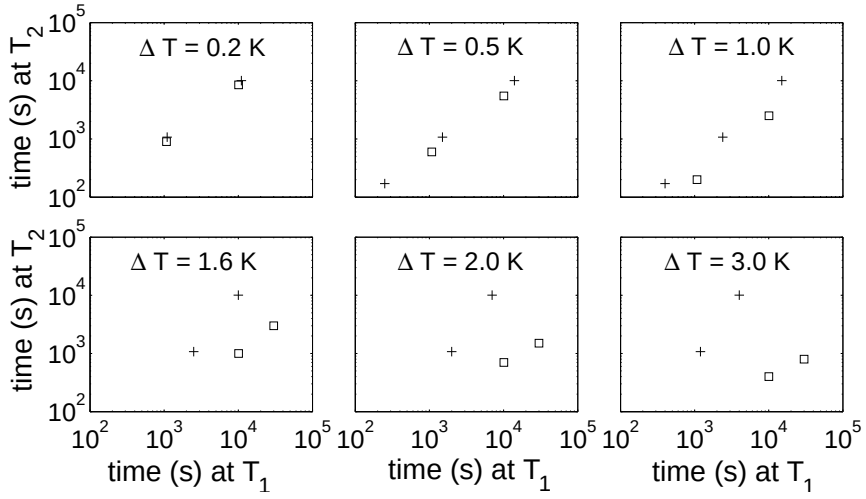

Figure 3.9: Relation between $t_{\rm w}$ and $t_{\rm eff}$ in twin-experiments – (T_1, T_2) shown as squares and (T_2, T_1) shown as pluses – on the $Fe_{0.50}Mn_{0.50}TiO_3$ sample. $T_1 = (19 - \Delta T)$ K and $T_2 = 19$ K with ΔT=0.2, 0.5, 1.0, 1.6, 2.0 and 3.0 K.

For the Ising spin glass, $\theta \approx 0.2$ imposing $\zeta \approx 1$. Hence, the observation that the $Fe_{0.50}Mn_{0.50}TiO_3$ spin glass seems less chaotic than the **Ag**Mn spin glass is consistent with the droplet model, although it is still an open question if the non-accumulative ageing can be described by the droplet model for the $Fe_{0.50}Mn_{0.50}TiO_3$ sample.

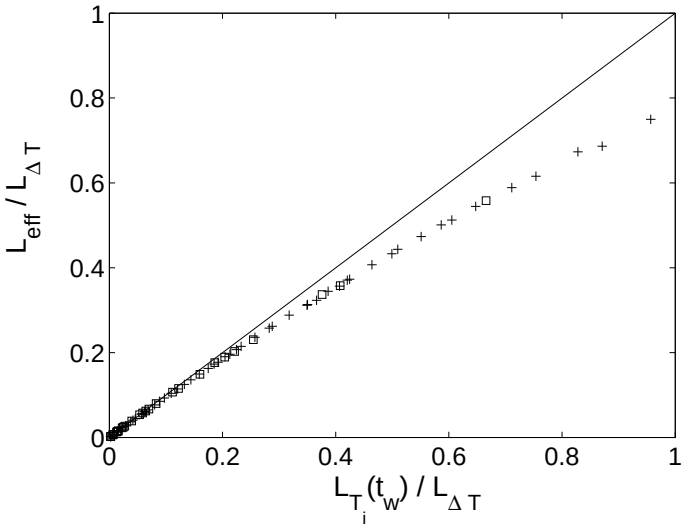

Figure 3.10: Scaling plot of $L_{\rm eff}/L_{\Delta \rm T}$ with $L_{\Delta \rm T} = (c\Delta T/J)^{-2.6}$ with $c = 8$ for the **Ag**Mn sample. The solid straight line represents the case of fully accumulative ageing. Pluses mark data with $T_i > T_m$ and squares data with $T_i < T_m$.

Memory

To further investigate memory and rejuvenation effects, we have performed T-cycling experiments: The sample is cooled from the paramagnetic phase to a temperature T_m within the spin-glass phase, at which it is aged a time t_{w_1}. The temperature is changed to $T_m - \Delta T$ for a time t_{w_2}, finally the temperature is shifted back to T_m where the ZFC relaxation is measured. Such experiments, performed on the **Ag**Mn sample with $T_m = 30$ K, $t_{\mathrm{w}_2} = 3000$ s and $T_m - \Delta T = 29$ K, are shown in Fig. 3.11. On the time scales probed in the experiments there is no overlap between the equilibrium domain configurations at these two temperatures. A memory of the first ageing at T_m is kept by the system, as evidenced by the peak in $S(t)$ at $t = t_{\mathrm{w}_1}$. However, there is also a second peak in $S(t)$ at short time scales indicating that the domain structure grown at 30 K has been partly erased at short length scales due to the ageing at 29 K. As seen from the figure, there is a continuous growth (decrease) of the peak at short times (long times) with increasing t_{w_2}. We can conclude that the ageing at the lower temperature can erase the domain structure grown at a higher temperature completely, only if the coherence length at the lower temperature $[L_{T_m+\Delta T}(t_{\mathrm{w}_2})]$ becomes similar in size to the coherence length attained at the higher temperature $[L_{T_m}(t_{\mathrm{w}_1})]$.

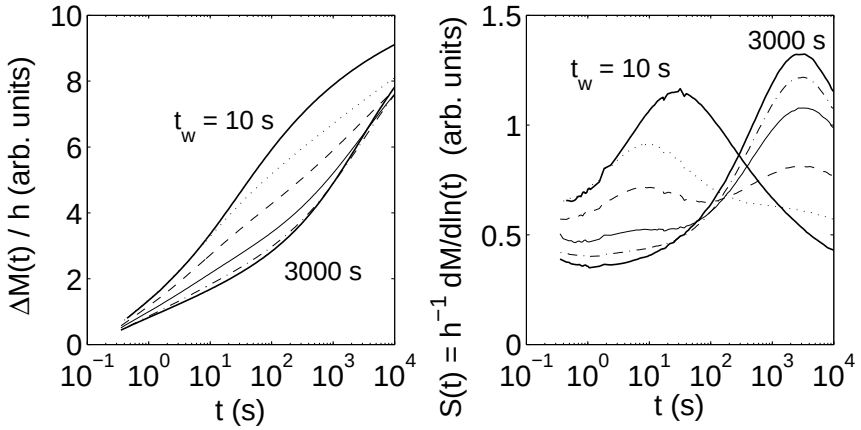

Figure 3.11: (a) ZFC susceptibility and (b) relaxation rate vs time for the **Ag**Mn sample. T-cycling experiments with $T_m = 30$ K, $t_{w_1} = 3000$ s, $T_m + \Delta T = 29$ K and $t_{w_2} = 30$ s (dash-dotted line), 300 s (solid line), 3000 s (dashed line) and 30 000 s (dotted line) are shown. The thick solid lines show ordinary ZFC-relaxation measurements with $t_w = 10$ s (a time allowing thermal stabilisation at T_m) and 3000 s.

Chapter 4

Magnetic single-domain nanoparticles

4.1 Introduction

The study of single-domain magnetic particles has been an active field of research since the pioneering work of Stoner and Wohlfarth [2], who studied the hysteretic rotation of the magnetisation over the magnetic-anisotropy energy barrier under the influence of an applied field, and Néel [3] who predicted that at non-zero temperature the magnetisation can surmount the energy barrier as a result of thermal agitation.

The theoretically most well studied systems are non-interacting classical spins (representing the magnetisation of the nanoparticles) with axially symmetric potentials (representing the magnetic anisotropy). A great step forward to compare experiments and theory was taken when measurements on individual particles were reported [87]. A profound knowledge of the physical properties of isolated particles is a prerequisite for further studies on e.g. quantum tunnelling in molecular nanomagnets or dipole-dipole interaction in dense samples.

In this thesis, the main interest is devoted to how dipolar interaction affects the physical properties of nanoparticle systems. Dipolar interaction is, due to its long range and reduced symmetry, difficult to treat analytically; most work on dipolar interaction is therefore numerical [88, 89, 90, 91]. Here we will use thermodynamic perturbation theory to treat weak dipolar interaction analytically. It will be shown that dipolar interaction can change the physical properties of an ensemble of particles considerably compared to those of the non-interacting system. In the next chapter we show that strongly interacting particle systems exhibit spin-glass-like properties.

Throughout this chapter we will for notational simplicity assume that the parameters characterising different nanoparticles are identical in analytical expressions. In real particle systems this is not the case, and Paper VI gives an example on how the polydispersivity of a real particle system can be taken into

account when comparing theory and experiments.

4.2 Basic properties

The current studies of magnetic single-domain nanoparticles are limited to systems where the particles are fixed in space (realised e.g. in frozen ferrofluids, single crystals of molecular magnets and magnetic nanoparticles in a solid matrix). We will also assume that every single-domain nanoparticle is in internal thermodynamic equilibrium and that its constituent spins rotate coherently. Moreover, we are only considering temperatures much lower than the Curie temperature, so the spontaneous magnetisation is approximately constant with temperature. Hence, the only relevant degree of freedom is the *orientation* of the net magnetic moment.

The Hamiltonian of a non-interacting nanoparticle consists of the magnetic anisotropy (which creates preferential directions of the magnetic moment orientation) and the Zeeman energy (which is the interaction energy between the magnetic moment and an external field). The nanoparticles are supposed to be well separated by a non-conductive medium (which can be obtained e.g. by adding a surfactant to a ferrofluid), and the only relevant inter-particle interaction mechanism is therefore dipole-dipole interaction.

4.2.1 Magnetic anisotropy

The term magnetic anisotropy is used to describe the dependence of the internal energy on the direction of the spontaneous magnetisation, creating "easy" and "hard" directions of magnetisation. In general, a bulk sample of a ferromagnet will exhibit magnetic anisotropy with the same symmetry as the crystal structure. This anisotropy energy originates from spin-orbit coupling and is called *magnetocrystalline anisotropy* [92]. The two most common symmetries are uniaxial and cubic. For uniaxial symmetry the energy is given by

$$E_a^{\text{uni}} = K_1 V \sin^2\theta + K_2 V \sin^4\theta + \cdots , \tag{4.1}$$

where V is the particle volume, K_1 and K_2 are anisotropy constants and θ is the angle between the magnetic moment and the symmetry axis. For cubic symmetry the anisotropy can be expressed in terms of the direction cosines (α_i) as

$$E_a^{\text{cubic}} = K_1 V(\alpha_1^2\alpha_2^2 + \alpha_2^2\alpha_3^2 + \alpha_3^2\alpha_1^2) + K_2 V \alpha_1^2\alpha_2^2\alpha_3^2 + \cdots , \tag{4.2}$$

where the α_i are defined through $\alpha_1 = \sin\theta\cos\phi$, $\alpha_2 = \sin\theta\sin\phi$ and $\alpha_3 = \cos\theta$, θ is the angle between the magnetisation and the z-axis and ϕ is the azimuthal angle.

For a single-domain ferromagnet, any non-spherical particle shape will give rise to *shape anisotropy* due to the internal magnetostatic energy. The magnetostatic energy, for an ellipsoid of revolution, is equal to

$$E_m = \tfrac{1}{2}\mu_0 V M_s^2 (N_z \cos^2\theta + N_x \sin^2\theta), \tag{4.3}$$

where θ is the angle between the magnetic moment and the polar axis $\hat{z}$, M_s is the saturation magnetisation, N_z is the demagnetisation factor along the polar axis and $N_x = N_y$ the demagnetisation factor along an equatorial axis. Both the magnetostatic energy for an ellipsoid and the uniaxial magnetocrystalline anisotropy energy [Eq. (4.1)] can to first order, except for a constant term, be written as

$$E_a = -A\cos^2\theta\,, \tag{4.4}$$

where $A = KV$ is the anisotropy energy barrier and the uniaxial anisotropy constant $K = \frac{1}{2}\mu_0 M_s^2(N_x - N_z)$ in the case of shape anisotropy. For a prolate ellipsoid, $K > 0$ and the anisotropy is of *easy axis* type, since there exist two minima of the anisotropy energy along $\pm\hat{z}$ (the anisotropy axis). For an oblate ellipsoid, $K < 0$ and the anisotropy energy has its minimum in the whole xy plane. In this case the anisotropy is of *easy plane* type.

With decreasing particle size, the magnetic contributions from the surface will eventually become more important than those from the bulk of the particle, and hence *surface anisotropy* energy will dominate over the magnetocrystalline anisotropy and magnetostatic energies. A uniaxial anisotropy energy proportional to the particle surface S,

$$E_a^{\text{surface}} = K_s S\cos^2\theta \tag{4.5}$$

has been observed experimentally by ferromagnetic resonance [93].

Hereafter, we will assume uniaxial anisotropy, of easy-axis type, given by Eq. (4.4) (if not otherwise indicated), since it is the simplest symmetry, but still it contains the basic elements (potential minima, barriers) responsible for the important role of magnetic anisotropy in superparamagnets. Experimental evidence for uniaxial anisotropy is given in Ref. [93, 94].

4.2.2 Superparamagnetic relaxation

The uniaxial anisotropy energy creates two potential wells separated by the energy barrier A. The magnetic moment is subjected to thermal fluctuations and may undergo a Brownian-type rotation surmounting the potential barriers. This relaxation process was proposed and studied by Néel in 1949 [3] and further developed by Brown in 1963 [95]. In the high potential barrier range, $\beta A \gg 1$, where $\beta = 1/k_B T$, the characteristic time for the overbarrier rotation τ can approximately be written in the Arrhenius form

$$\tau \simeq \tau_0 \exp(\beta A)\,, \tag{4.6}$$

where $\tau_0 \sim 10^{-9} - 10^{-12}$ s. For observation times t_{obs} much longer than the relaxation time, $\vec{m}$ maintains the thermal-equilibrium distribution of orientations as in a classical paramagnet - but due to the much larger magnetic moment than a single spin, this phenomenon was called *superparamagnetism* [96]. The condition of superparamagnetism ($t_{\text{obs}} \gg \tau$) corresponds to a temperature range that fulfils, $\ln(t_{\text{obs}}/\tau_0) > \beta A$. For $t_{\text{obs}} \sim 10$ s, due to the small value of τ_0, this equilibrium range extends down to low thermal energies compared

to the anisotropy energy ($25 > \beta A$). Hence, *within the equilibrium regime*, the system displays an isotropic behaviour at high temperatures ($\beta A \ll 1$), but a strongly anisotropic behaviour at low temperatures ($\beta A \gg 1$) with a Heisenberg to Ising crossover in-between.

If $t_{\rm obs} \ll \tau$, the magnetic moment is *blocked* in one of the potential wells. A state which corresponds to stable magnetisation in a bulk magnet. If the measurement time is of the same order as the relaxation time ($t_{\rm obs} \sim \tau$), dynamical time dependent effects are observed.

4.2.3 Effects of a magnetic field

The Hamiltonian of a noninteracting nanoparticle with uniaxial anisotropy is given by,

$$\mathcal{H} = -\frac{A}{m^2}(\vec{m}\cdot\vec{n})^2 - \mu_0 \vec{m}\cdot\vec{H} \tag{4.7}$$

where $\vec{m}$ is the magnetic moment with $m = M_{\rm s}V$, $A = KV$ and $\vec{n}$ is a unit vector along the symmetry axis of the anisotropy energy (anisotropy direction). By introducing unit vectors for the magnetic moment ($\vec{s} = \vec{m}/m$) and the external magnetic field ($\hat{h} = \vec{H}/H$) and defining dimensionless parameters for the anisotropy and magnetic field,

$$\sigma = \beta A, \qquad \xi = \beta \mu_0 m H, \tag{4.8}$$

we can write a dimensionless Hamiltonian as,

$$-\beta\mathcal{H} = \sigma(\vec{s}\cdot\vec{n})^2 + \xi(\vec{s}\cdot\hat{h}). \tag{4.9}$$

The bistable character of the zero-field Hamiltonian will be destroyed by a sufficiently large field. The critical field for $\vec{n}\|\hat{h}$ is called *anisotropy field*, and is given by

$$H_K = \frac{2A}{\mu_0 m} = \frac{2K}{\mu_0 M_{\rm s}}. \tag{4.10}$$

We can define another dimensionless field quantity:

$$h = \frac{H}{H_K} = \frac{\xi}{2\sigma}\ , \tag{4.11}$$

which is the field measured in units of the anisotropy field. The Hamiltonian, as a function of the angle θ between the anisotropy axis and the magnetic moment ($\vec{s}\cdot\vec{n} = \cos\theta$), is shown in Fig. 4.1 for different values of the longitudinal field.

4.2.4 Inter-particle interaction

Dipole-dipole interaction is ubiquitous in magnetic spin systems, but usually other interaction mechanisms (e.g. exchange interaction) dominate. The relative weakness of the dipolar coupling between magnetic ions in paramagnetic systems results in characteristic temperatures lying in the range of 0.01-0.1 K. For superparamagnetic nanoparticles (for which care has been taken to avoid

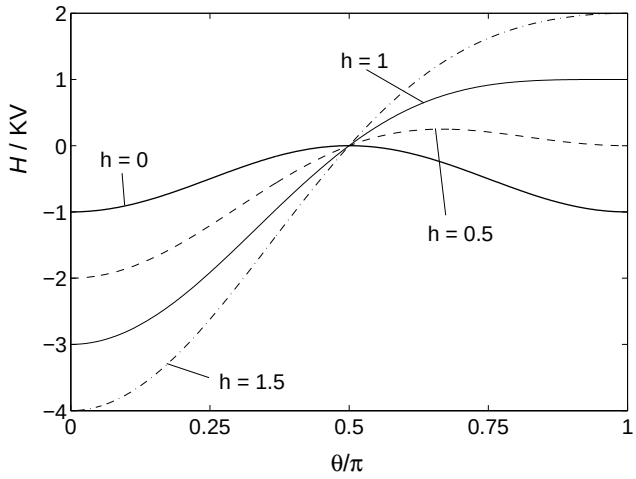

Figure 4.1: Magnetic energy vs θ in the case of longitudinal field for different values of the reduced field $h = H/H_K$.

direct contact between the particles) exchange interaction and other interaction mechanisms can usually be discarded so that the dipolar interaction is the only relevant interparticle interaction. In addition, the size of the typical magnetic moment ($S \sim 10^2 - 10^5$ magnetic spins) shifts the relevant temperatures up to the range of a few Kelvin, making it possible to observe effects of dipolar interaction in conventional magnetisation experiments.

The dipolar field, created by all other spins, at the position $\vec{r}_i$ of the spin $\vec{s}_i$, is given by

$$\vec{H}_i = \frac{m}{4\pi a^3} \sum_j \mathbf{G}_{ij} \cdot \vec{s}_j \,, \tag{4.12}$$

where the term $j = i$ is omitted from the summation, a is defined in such a way that a^3 is the mean volume around each spin, and

$$\mathbf{G}_{ij} = \frac{1}{r_{ij}^3} \left(3\,\hat{r}_{ij}\hat{r}_{ij} - \mathbf{1}\right), \tag{4.13}$$

$$\vec{r}_{ij} = \vec{r}_i - \vec{r}_j, \quad \hat{r}_{ij} = \vec{r}_{ij}/r_{ij} \,, \tag{4.14}$$

where $\mathbf{1}$ is the unit tensor.

By introducing the dimensionless coupling constant

$$\xi_{\mathrm{d}} = \frac{\mu_0 m^2}{4\pi a^3} \frac{1}{k_{\mathrm{B}} T} \,, \tag{4.15}$$

and noting that the dipolar energy $E_{\mathrm{d}} = \frac{\mu_0}{2} \sum_{i \neq j} \vec{m} \cdot \vec{H}_i$, we can write the total dimensionless Hamiltonian of an interacting nanoparticle system as

$$-\beta\mathcal{H} = \sigma \sum_i (\vec{s}_i \cdot \vec{n}_i)^2 + \xi \sum_i (\vec{s}_i \cdot \hat{h}) + \xi_{\mathrm{d}} \sum_{i>j} \omega_{ij} \,, \tag{4.16}$$

where $\omega_{ij} = \vec{s}_i \cdot \mathbf{G}_{ij} \cdot \vec{s}_j$. Note that the interaction strength can also be measured by the temperature independent coupling parameter

$$h_{\rm d} = \xi_{\rm d}/2\sigma = \frac{M_{\rm s}}{4\pi H_K} c \,, \tag{4.17}$$

which is the magnitude of the field, measured in units of the anisotropy field H_K, produced at a given position by a dipole at a distance a. Here, $c = V/a^3$ is the volume concentration of particles.

Dipole-dipole interaction is long-ranged and anisotropic, which makes it cumbersome to treat both analytically and numerically. For a system with randomness in particle positions and anisotropy directions, the dipolar interaction introduces frustration and disorder leading to glassy dynamics for strongly interacting systems [97]. We will therefore only use analytical and numerical treatment for weakly interacting particle systems, while strongly interacting systems will be discussed in terms of collective spin-glass behaviour in chapter 5.

4.3 Thermal equilibrium properties

We will here calculate some thermodynamic quantities for independent and weakly interacting nanoparticles. The thermal-equilibrium average of any quantity $B(\vec{s}_1, \ldots, \vec{s}_N)$ is given by

$$\langle B \rangle = \frac{1}{\mathcal{Z}} \int d\Gamma B \, \exp(-\beta \mathcal{H}) \,, \tag{4.18}$$

where $\mathcal{Z} = \int d\Gamma \exp(-\beta\mathcal{H})$ is the partition function. For classical spins the different states correspond to different spin orientations so that $d\Gamma = \prod_i d\Omega_i$, with $d\Omega_i = d^2\vec{s}_i/2\pi$.

4.3.1 Linear and non-linear susceptibility of superparamagnets with a general anisotropy energy

We will consider the linear and non-linear susceptibilities of superparamagnets. For the calculation of other thermodynamic quantities of independent nanoparticles, see e.g. the review by García-Palacios [98]. The non-linear susceptibilities can constitute more sensitive tools to investigate static and dynamic properties of magnetic nanoparticles than the linear susceptibility. A common experimental situation is an ensemble of nanoparticles with the anisotropy axes oriented randomly (e.g. frozen ferrofluids). This randomness may obscure the possibility to extract information about the intrinsic properties of the nanoparticles (e.g. the anisotropy).

A case that has already been studied is nanoparticles with uniaxial anisotropy and random anisotropy orientations [99, 100]: The static *linear* susceptibility is equal to that of isotropic spins $\chi_{\rm iso} = \frac{1}{3}\beta\mu_0 m^2$, while the static *nonlinear* susceptibility has an additional anisotropy induced temperature dependence

compared to isotropic superparamagnets, $\chi^{(3)}_{\rm iso} = -\frac{1}{45}\beta^3\mu_0^3 m^4$ [99]. It is important to know the origin of such a deviation from the common $1/T^3$ behaviour in order not to mix it up with deviations due to interaction or quantum effects.

In Paper VII we have studied the linear and nonlinear equilibrium response of ensembles of spins in which the anisotropy axes are distributed at random. The analysis is restricted to independent spins with Hamiltonians having inversion symmetry [$\mathcal{H}(\vec{m}) = \mathcal{H}(-\vec{m})$]. The method is valid for any kind of anisotropy, but if a bias field is applied in addition to the probing field the condition of inversion symmetry breaks down.

Linear susceptibility

The effective linear susceptibility, averaged over random anisotropy directions, reads

$$\overline{\chi} = \frac{1}{3}\beta\mu_0 m^2\,, \tag{4.19}$$

where all vestiges of the magnetic anisotropy have disappeared. Since the result is valid for any kind of anisotropy, $\overline{\chi}$ can not be used to extract any information about the anisotropy energy.

Nonlinear susceptibility

The effective nonlinear susceptibility, averaged over random anisotropy, can be written

$$\bar{\chi}^{(3)} = -\frac{1}{15}\beta^3\mu_0^3 m^4[\langle x^2\rangle + \langle y^2\rangle + \langle z^2\rangle]^2\,, \tag{4.20}$$

where the anisotropy dependence remains after the random averaging and is contained in the statistical-mechanical averages. By introducing

$$S_2 = \tfrac{1}{2}(3\langle z^2\rangle - 1)\,, \qquad \Delta = \tfrac{1}{2}(\langle y^2\rangle - \langle x^2\rangle)\,, \tag{4.21}$$

we can finally write the nonlinear susceptibility as

$$\bar{\chi}^{(3)} = -\frac{1}{45}\beta^3\mu_0^3 m^4(1 + 2S_2^2 + 6\Delta^2)\,. \tag{4.22}$$

For *isotropic* spins as well as for spins with *cubic* anisotropy, $\langle x^2\rangle = \langle y^2\rangle = \langle z^2\rangle = 1/3$ and hence

$$\bar{\chi}^{(3)}_{\rm cubic} = \bar{\chi}^{(3)}_{\rm iso} = -\tfrac{1}{45}\beta^3\mu_0^3 m^4\,. \tag{4.23}$$

For spins with axially symmetric anisotropy $\langle x^2\rangle = \langle y^2\rangle$ and hence $\Delta = 0$. Properties of S_2 in the case of uniaxial anisotropy are discussed in the appendix. By using the asymptotic values for S_2 we can see that $\bar{\chi}^{(3)}_{\rm uni}$ must exhibit a crossover from the high-temperature isotropic regime ($\langle z^2\rangle = 1/3$) to the low-temperature Ising ($\langle z^2\rangle = 1$) or planar-rotor ($\langle z^2\rangle = 0$) regimes, so that [99,

100]

$$\begin{aligned}
\bar{\chi}^{(3)}_{\text{uni}} &\simeq -\tfrac{1}{45}\beta^3\mu_0^3 m^4 \qquad \text{(high } T\text{)}, \\
\bar{\chi}^{(3)}_{\text{uni}} &\simeq -\tfrac{1}{15}\beta^3\mu_0^3 m^4 \qquad \text{(low } T\text{, easy-axis)}, \\
\bar{\chi}^{(3)}_{\text{uni}} &\simeq -\tfrac{1}{30}\beta^3\mu_0^3 m^4 \qquad \text{(low } T\text{, easy-plane)}.
\end{aligned} \tag{4.24}$$

Equation (4.22) can be used to calculate the static susceptibility for more complicated functional forms of the anisotropy, e.g. biaxial, as was done in Paper VII.

4.3.2 Thermodynamic perturbation theory for weakly interacting superparamagnets

We will consider dipolar interaction in zero field so that the total Hamiltonian is given by the sum of the anisotropy and dipolar energies $\mathcal{H} = E_{\text{a}} + E_{\text{d}}$. By restricting the calculation of thermal-equilibrium properties to the case $\xi_{\text{d}} \ll 1$, we can use thermodynamical perturbation theory [101, 102] to expand the Boltzmann distribution in powers of ξ_{d}. As is shown in Paper VIII, this leads to an expression of the form

$$W = W_{\text{a}}\left(1 + \xi_{\text{d}}F_1 + \tfrac{1}{2}\xi_{\text{d}}^2 F_2 + \cdots\right) , \tag{4.25}$$

where F_1 is linear in E_{d} and F_2 is (up to) quadratic in E_{d}, while

$$W_{\text{a}} = \mathcal{Z}_a^{-1}\exp(-\beta E_{\text{a}}) , \tag{4.26}$$

is the Boltzmann distribution of the noninteracting ensemble. By keeping all averages weighted with W_{a}, the thermal-equilibrium quantities calculated with this method will be exact in the anisotropy and only perturbational in the dipolar interaction.[1] An ordinary high-temperature expansion corresponds to expanding Eq. (4.26) further in powers of β.

Linear susceptibility

We can obtain the equilibrium linear susceptibility using Eq. (2.8). If, in addition, there is no external *bias* field applied, the susceptibility is simply given by

$$\chi = \frac{\mu_0 m^2}{k_{\text{B}}T}\frac{1}{N}\langle s_z^2\rangle, \qquad s_z = \sum_i (\vec{s}_i \cdot \hat{h}), \tag{4.27}$$

where $\hat{h}$ is a unit vector along the probing field direction and s_z is the field projection of the net magnetic moment. Calculating $\langle s_z^2\rangle$ using thermodynamic perturbation theory yields an expansion of the susceptibility of the form

$$\chi = \frac{\mu_0 m^2}{k_{\text{B}}T}\left(a_0 + \xi_{\text{d}}a_1 + \tfrac{1}{2}\xi_{\text{d}}^2 a_2\right) , \tag{4.28}$$

[1] A similar approach was recently used by B. Huke and M. Lücke [103]. They performed a "Born–Mayer" expansion to study the field-dependent magnetisation of a ferrofluid. As the magnetic anisotropy was not included, their noninteracting distribution corresponded to the Zeeman energy; $W_{\text{a}} \propto \exp(\vec{s}\cdot\vec{\xi})$.

with the general expressions for the coefficients a_n given in Appendix B of Paper VIII. Simplified expressions for the coefficients can be obtained for some orientational distributions of the anisotropy axes, e.g. parallel anisotropy axes and randomly distributed axes.

For systems with parallel axes (e.g., single crystals of magnetic molecular clusters or a ferrofluid frozen in a strong field), the coefficients for the longitudinal response read

$$a_{0,\parallel} = \frac{1+2S_2}{3} \tag{4.29}$$

$$a_{1,\parallel} = \frac{1+4S_2+4S_2^2}{9}\,\mathcal{C}\,, \tag{4.30}$$

$$\begin{aligned}\tfrac{1}{2}a_{2,\parallel} &= -\frac{1+4S_2+4S_2^2}{27}\left[(1-S_2)\left(\bar{\mathcal{R}}-\mathcal{S}\right)+3S_2\,\left(\mathcal{T}-\mathcal{U}\right)\right] \\ &\quad+\frac{7+10S_2-35S_2^2+18S_4}{315}\left[(1-S_2)\left(\bar{\mathcal{R}}-\mathcal{R}\right)+3S_2\left(\mathcal{T}-\tfrac{1}{3}\bar{\mathcal{R}}\right)\right]\,,\end{aligned} \tag{4.31}$$

where $\mathcal{C}$, $\mathcal{R}$ ($\bar{\mathcal{R}}$), $\mathcal{S}$, $\mathcal{T}$ and $\mathcal{U}$ are certain *lattice sums* whose properties are discussed below in Sec. 4.3.3. The properties of $S_l(\sigma)$ are discussed in the appendix.

To obtain the susceptibility when the anisotropy axes are distributed at random, we average the general expressions for the a_n over $\vec{n}$, getting

$$a_{0,\mathrm{ran}} = \frac{1}{3} \tag{4.32}$$

$$a_{1,\mathrm{ran}} = \frac{1}{9}\,\mathcal{C} \tag{4.33}$$

$$\tfrac{1}{2}a_{2,\mathrm{ran}} = -\frac{1}{27}\left(\bar{\mathcal{R}}-\mathcal{S}\right)+\frac{1}{45}\,(1-S_2^2)\,(\bar{\mathcal{R}}-\mathcal{R})\,. \tag{4.34}$$

Note that in the limit of isotropic spins (where $S_l \to 0$) the results for coherent axes and for random anisotropy duly coincide and agree with ordinary high-temperature expansions.

Specific heat

The specific heat at constant volume can be obtained directly from $\mathcal{Z}$ using Eq. (2.6):

$$\frac{c_v}{k_\mathrm{B}} = \beta^2\frac{\partial^2}{\partial\beta^2}(\ln\mathcal{Z}) = \sigma^2\frac{\partial^2}{\partial\sigma^2}(\ln\mathcal{Z})\,, \tag{4.35}$$

where, to take the σ-derivative, the coupling parameter ξ_d is expressed as $\xi_\mathrm{d} = 2\sigma h_\mathrm{d}$ [Eq. (4.17)]. As in the calculation of χ, we only consider the zero-field specific heat. In that case, the term linear in ξ_d vanishes and the expansion of the specific heat to second order in ξ_d reads,

$$\frac{c_v}{Nk_\mathrm{B}} = \sigma^2 b_0 + \tfrac{1}{2}\xi_\mathrm{d}^2 b_2\,, \tag{4.36}$$

where the zeroth order coefficient

$$b_0 = \frac{4}{315}(18S_4 - 35S_2^2 + 10S_2 + 7)\,, \tag{4.37}$$

gives the specific heat in the absence of interaction [98]. The general formula for b_2 is given in Appendix C of Paper VIII. Again, it is possible to obtain simplified formulae for coherent anisotropy axes and for random anisotropy. In the first case ($\vec{n}_i = \vec{n}$, $\forall i$) we obtain

$$\begin{aligned} b_{2,\parallel} &= \tfrac{1}{3}\Big\{1 - S_2^2 - 4\sigma S_2 S_2' - \sigma^2[S_2 S_2'' + (S_2')^2]\Big\}\mathcal{R} \\ &\quad + \tfrac{1}{3}\Big(2S_2(1-S_2) + 4\sigma S_2'(1-2S_2) \\ &\qquad + \sigma^2\{S_2'' - 2[S_2 S_2'' + (S_2')^2]\}\Big)(\bar{\mathcal{R}} - \mathcal{R}) \\ &\quad + \Big\{S_2^2 + 4\sigma S_2 S_2' + \sigma^2[S_2 S_2'' + (S_2')^2]\Big\}\mathcal{T}\,, \end{aligned} \tag{4.38}$$

where $S_2' = dS_2/d\sigma$. For randomly distributed axes, on averaging the general expression for b_2 over $\vec{n}$, one simply gets

$$b_{2,\mathrm{ran}} = \tfrac{1}{3}\mathcal{R}. \tag{4.39}$$

This is the same correction term as that obtained for *isotropic* spins by Waller [104] and Van Vleck [105] using ordinary high-temperature expansions.

Dipolar fields

We are interested in calculating thermodynamical averages of the dipolar field, to introduce them in the expression for the relaxation rate in a weak but arbitrary oriented field, in order to obtain an expression for the relaxation rate of weakly interacting dipoles (we will argue in Sec. 4.4.3 that the effect of weak dipolar interaction can be accounted for by the thermodynamic averages of the dipolar field). Since the uniaxial anisotropy has inversion symmetry, only the square of the field will enter the low field expression for the relaxation rate and not the field itself. In addition, the effects of longitudinal and transversal fields will be different. In Paper IX we calculated $\langle \xi_{i,\parallel}^2 \rangle$ and $\langle \xi_{i,\perp}^2 \rangle = \langle \xi_i^2 \rangle - \langle \xi_{i,\parallel}^2 \rangle$ to second order in ξ_d. If we consider infinite systems, the index i can be removed since all spins have the same surroundings. For a system with aligned anisotropy axes the averaged fields are given in terms of the lattice sums by

$$\begin{aligned} \langle \xi_\parallel^2 \rangle &= \frac{\xi_\mathrm{d}^2}{3}\left[(1-S_2)\,\bar{\mathcal{R}} + 3S_2\,\mathcal{T}\right], \\ \langle \xi_\perp^2 \rangle &= \frac{\xi_\mathrm{d}^2}{3}\left[3\mathcal{R} - (1-S_2)\bar{\mathcal{R}} + 3S_2\,(\mathcal{R} - \bar{\mathcal{R}} - \mathcal{T})\right]\,, \end{aligned} \tag{4.40}$$

while for randomly distributed anisotropy axes they read

$$\overline{\langle \xi_\parallel^2 \rangle} = \frac{\xi_\mathrm{d}^2}{3}\mathcal{R}\,, \qquad \overline{\langle \xi_\perp^2 \rangle} = \frac{\xi_\mathrm{d}^2}{3}2\mathcal{R}\,. \tag{4.41}$$

Note that the result for random anisotropy is identical to the result for isotropic dipoles.

4.3.3 The lattice sums

An essential element of the expressions derived for χ, c_v, and the dipolar fields are the following "lattice sums"[2]

$$\mathcal{C} = \frac{1}{N}\sum_i \sum_{j\neq i} \hat{h}\cdot\mathbf{G}_{ij}\cdot\hat{h} \tag{4.42}$$

$$\mathcal{R} = \frac{2}{N}\sum_i \sum_{j\neq i} r_{ij}^{-6} \tag{4.43}$$

$$\bar{\mathcal{R}} = \frac{1}{N}\sum_i \sum_{j\neq i} \hat{h}\cdot\mathbf{G}_{ij}\cdot\mathbf{G}_{ij}\cdot\hat{h} \tag{4.44}$$

$$\mathcal{S} = \frac{1}{N}\sum_i \sum_{j\neq i} \sum_{k\neq j} \hat{h}\cdot\mathbf{G}_{ij}\cdot\mathbf{G}_{jk}\cdot\hat{h} \tag{4.45}$$

$$\mathcal{T} = \frac{1}{N}\sum_i \sum_{j\neq i} (\hat{h}\cdot\mathbf{G}_{ij}\cdot\hat{h})^2 \tag{4.46}$$

$$\mathcal{U} = \frac{1}{N}\sum_i \sum_{j\neq i} \sum_{k\neq j} (\hat{h}\cdot\mathbf{G}_{ij}\cdot\hat{h})(\hat{h}\cdot\mathbf{G}_{jk}\cdot\hat{h}) \tag{4.47}$$

The long range of the dipole-dipole interaction leads to a shape dependence of the physical quantities in an external magnetic field [106, 107], and hence on the linear susceptibility (which is a field derivative), but not the zero-field specific heat or the dipolar fields. In the expressions obtained for the susceptibility, this shape dependence is borne by the slowly convergent lattice sums $\mathcal{C}$, $\mathcal{S}$ and $\mathcal{U}$. If we consider "sufficiently isotropic" lattices, in the sense of fulfilling $\sum(r_x)^n = \sum(r_y)^n = \sum(r_z)^n$, e.g. cubic and completely disordered lattices (incidentally, the type of arrangements for which in the classical Lorentz cavity-field calculation the contribution of the dipoles inside the "small sphere" vanishes) these lattice sums vanish for large spherical samples. The sums $\mathcal{R}$, $\bar{\mathcal{R}}$ and $\mathcal{T}$ on the other hand contain r_{ij}^{-6} which make them rapidly convergent and shape independent. For sufficiently symmetric lattices $\bar{\mathcal{R}} = \mathcal{R} = 16.8,\ 14.5,\ 14.5$ for simple cubic, bcc and fcc structures [108], and $\mathcal{T} = 13.54$ (sc), 3.7 (bcc), 4.3 (fcc). Note that since $\bar{\mathcal{R}} - \mathcal{R} = 0$, some terms vanish in the above expressions for χ, c_v, and the dipolar fields.

Shape and anisotropy dependence

For the linear susceptibility, the zero-field specific heat as well as the dipolar fields, the anisotropy dependence cancels out in the case of random anisotropy (at least for sufficiently symmetric lattices). In other cases the anisotropy is a very important parameter as shown in Paper VIII. The specific heat for uncoupled spins does not depend on the orientations of the anisotropy axes, however the corrections due to the dipolar coupling do (see Fig. 4.2). The shape dependence of the linear susceptibility is illustrated in Fig. 4.3. The susceptibility

[2] $\hat{h}$ should be replaced by $\vec{n}$ in the formulae for c_v and the dipolar fields.

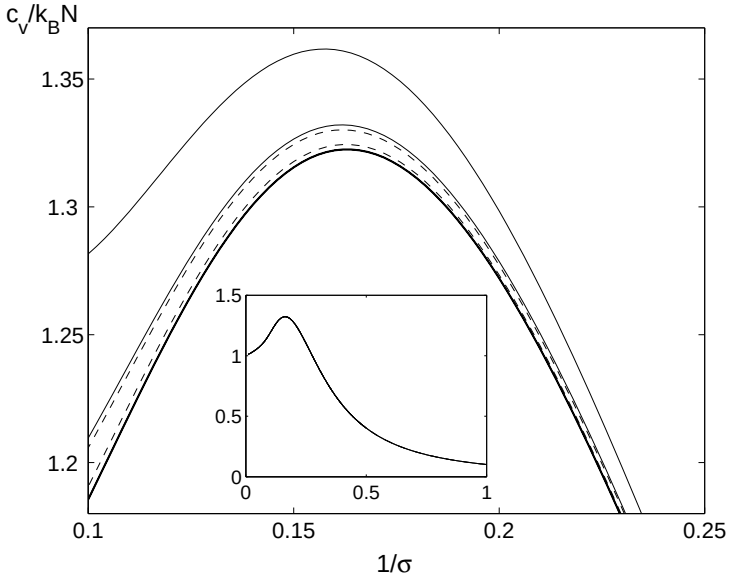

Figure 4.2: The specific heat per spin vs temperature for non-interacting spins (thick line), and weakly interacting spins with randomly distributed anisotropy axes (dashed lines) and parallel axes (thin lines) arranged on a simple cubic lattice. In each case, $h_\mathrm{d} = \xi_\mathrm{d}/2\sigma = 0.003$ and 0.006 from bottom to top. The inset shows the specific heat for non-interacting spins over a wider temperature interval.

is calculated for small systems using both thermodynamic perturbation theory and a Monte Carlo technique (see Appendix D of Paper VIII), taking the dipolar interaction into account without any approximation. It can be seen that χ obtained by thermodynamic perturbation theory accurately describes the simulated susceptibility at high temperatures, while the results start to deviate at the lowest temperatures displayed. An estimate of the lowest temperature attainable by the thermodynamic perturbation theory is $\xi_\mathrm{d} \sim 1/6$, which is milder than the *a priori* restriction $\xi_\mathrm{d} \ll 1$.

4.4 Dynamic properties

At high temperatures, a nanoparticle is in a superparamagnetic state with thermal-equilibrium properties as described in the previous section. At low enough temperatures, the magnetic moment is blocked in one potential well with a small probability to surmount the energy barrier, while at intermediate temperatures, where the relaxation time of a spin is comparable to the observation time, dynamical properties can be observed, e.g. magnetic relaxation and a frequency dependent ac susceptibility.

For applications such as magnetic recording media it is necessary to know how different parameters will affect the relaxation time in order to avoid spontaneous data erasure (caused by thermal fluctuations) on the lifetime of the

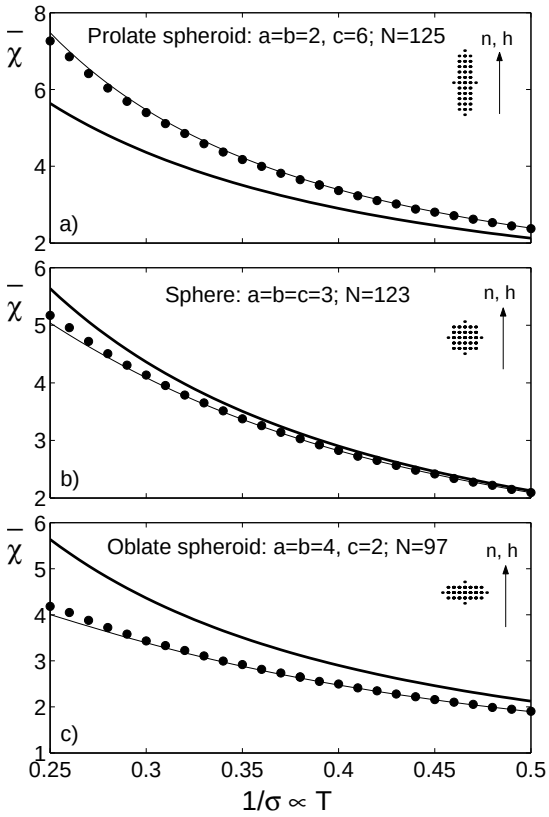

Figure 4.3: Equilibrium linear susceptibility in reduced units $\bar{\chi} = \chi(H_K/m)$ vs temperature for three different ellipsoidal systems with equation $x^2/a^2 + y^2/b^2 + z^2/c^2 \leq 1$, resulting in a system of N dipoles arranged on a simple cubic lattice. The points shown are the projection of the spins to the xz-plane. The probing field is applied along the anisotropy axes, which are parallel to the z axis. The thick lines indicate the equilibrium susceptibility of the corresponding noninteracting system (which does not depend on the shape of the system and is the same in the three panels); thin lines show the susceptibility including the corrections due to the dipolar interaction obtained by thermodynamic perturbation theory [Eq. (4.28)]; and the symbols represent the susceptibility obtained with a Monte Carlo method. The dipolar interaction strength is $h_{\rm d} = \xi_{\rm d}/2\sigma = 0.02$.

device. Due to the ongoing effort to increase the information/surface ratio it is of special importance to know how the dipolar interaction of densely packed nanoparticles will affect the relaxation time.

Brown derived in 1963 [95] the Fokker-Planck equation for the probability distribution of the spin orientation, starting from the stochastic Gilbert equation, and calculated the relaxation time for particles with uniaxial anisotropy in a longitudinal field. Recent work on spins with non-axially symmetric potential revealed a large dependence of the relaxation time on the damping coefficient λ in the medium-to-weak damping regime [109, 110, 111]. Experiments on indi-

vidual nanoparticles analysed with accurate asymptotes of the relaxation time [112], gave damping coefficients in the range: $\lambda \approx 0.05 - 0.5$. Non-axially symmetric potentials are for example created when applying a field at an oblique angle to a uniaxial spin. This oblique field can either be a bias field [113] or a non-linear probing field [114]. In the case of interacting particles a transverse field component arises from the dipolar field of the surrounding particles. This explains the dependence on λ of the blocking temperature that was first observed in numerical simulations by Berkov and Gorn [91] (see Fig. 4.4).

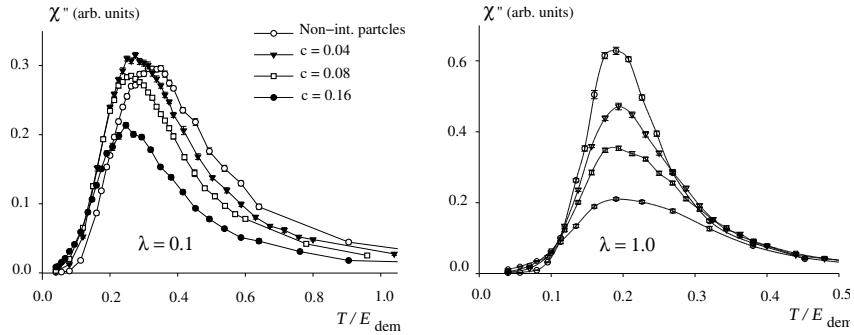

Figure 4.4: The out-of-phase component of the ac susceptibility versus temperature for two different values of the damping $\lambda = 0.1$ and 1.0. $\gamma M_{\rm s}\omega = 0.03$, $E_{\rm dem} = M_{\rm s}^2 V/k_{\rm B}$ and $h_{\rm d} = (\mu_0/4\pi)(c/\beta)$ with $\beta = 2.0$. From Ref. [91].

The importance of including the damping in models describing the dynamic response of spins with non-axially symmetric potentials (e.g. interacting uniaxial spins) tells us that models based only on how the energy-barriers change [115, 116] necessarily overlook the precession of the magnetic moment ($\lambda \to \infty$) and therefore cannot account for the numerical results of Berkov and Gorn. For this reason we developed an approach that includes the dependence on the precession (Paper VIII).

4.4.1 The equation of motion

We will here present the equation of motion for a classical spin (the magnetic moment of a ferromagnetic single-domain particle) in the context of the theory of stochastic processes. The basic Langevin equation is the stochastic Landau-Lifshitz(-Gilbert) equation [95, 117]. More details on this subject and on various techniques to solve this equation can be found in the reviews by Coffey et al. [118] and García-Palacios [98].

Deterministic equations

The motion of a magnetic moment can be described by the Gilbert equation [119]

$$\frac{1}{\gamma}\frac{d\vec{m}}{dt} = \vec{m} \times \vec{H}_{\rm eff} - \frac{\lambda}{\gamma m}\vec{m} \times \frac{d\vec{m}}{dt} \tag{4.48}$$

where γ is the gyromagnetic ratio (which includes μ_0), λ is a dimensionless damping coefficient, and the effective field is given by

$$\vec{H}_{\text{eff}} = -\mu_0^{-1}\partial\mathcal{H}/\partial\vec{m}\,. \tag{4.49}$$

The first term on the right-side of Eq. (4.48) represents the precession of the magnetic moment about the axis of the effective field, while the second one is the damping term, which rotates $\vec{m}$ towards the potential minima and is responsible for the dissipation of the energy.

The Gilbert equation can be cast into the Landau-Lifshitz form [120]

$$\frac{1}{\gamma}\frac{d\vec{m}}{dt} = \vec{m}\times\vec{H}_{\text{eff}} - \frac{\lambda}{m}\vec{m}\times(\vec{m}\times\vec{H}_{\text{eff}}) \tag{4.50}$$

with a "renormalised" gyromagnetic ratio $\gamma \to \gamma/(1+\lambda^2)$ (see e.g. [118, 98]).

In the case of uniaxial anisotropy and a Hamiltonian given by Eq. (4.7) $\vec{H}_{\text{eff}} = (H_K/m)(\vec{m}\cdot\vec{n})\vec{n} + \vec{H}$, where H_K is the anisotropy field and $\vec{H}$ is an external field. The ferromagntic resonance frequency ω for the precession about $\vec{H}_{\text{eff}}$ is given by $\omega = \gamma\mu_0 H_{\text{eff}}$ [121].

Stochastic equations

At $T \neq 0$ the magnetic moment will interact with the microscopic degrees of freedom (phonons, conducting electrons, nuclear spins etc.). The complexity of this interaction allows an idealisation, namely to introduce them through a stochastic model. The simplest model is the Brownian, in which the interaction of $\vec{m}$ with the surroundings is represented by a randomly fluctuating magnetic field. This fluctuating field is necessarily combined with a dissipation (damping) term and these two terms are linked by fluctuation-dissipation relations [122].

In the work of Brown [95] and Kubo and Hashitsume [117] the starting equation is the Gilbert equation (4.48), in which the effective field is increased by a fluctuating field yielding the stochastic Gilbert equation. This equation can, as in the deterministic case, be cast into the Landau-Lifshitz form as,

$$\frac{1}{\gamma}\frac{d\vec{m}}{dt} = \vec{m}\times[\vec{H}_{\text{eff}} + \vec{b}_{\text{fl}}(t)] - \frac{\lambda}{m}\vec{m}\times\{\vec{m}\times[\vec{H}_{\text{eff}} + \vec{b}_{\text{fl}}(t)]\}\,, \tag{4.51}$$

known as the stochastic Landau-Lifshitz-Gilbert (LLG) equation. The fluctuating field is assumed to be Gaussian distributed white noise,

$$\langle b_{\text{fl},\alpha}(t)\rangle = 0, \qquad \langle b_{\text{fl},\alpha}(t)b_{\text{fl},\beta}(t')\rangle = 2D\delta_{\alpha\beta}\delta(t-t')\,, \tag{4.52}$$

with $\alpha,\beta = x,y,z$. García-Palacios and Lázaro [123] showed that the stochastic Landau-Lifshitz-Gilbert equation (4.51) and the simpler stochastic Landau-Lifshitz (LL) equation,

$$\frac{1}{\gamma}\frac{d\vec{m}}{dt} = \vec{m}\times[\vec{H}_{\text{eff}} + \vec{b}_{\text{fl}}(t)] - \frac{\lambda}{m}\vec{m}\times(\vec{m}\times\vec{H}_{\text{eff}})\,, \tag{4.53}$$

both give rise to the same Fokker-Planck equation, describing the average properties of the magnetic moment, but with different Einstein-type relations between the amplitude of the fluctuating field and the temperature,

$$D_{\mathrm{LLG}} = \frac{\lambda}{1+\lambda^2}\frac{k_{\mathrm{B}}T}{\gamma m}, \qquad D_{\mathrm{LL}} = \lambda\frac{k_{\mathrm{B}}T}{\gamma m}\,. \tag{4.54}$$

4.4.2 Relaxation time in a weak but arbitrary field

We are interested in knowing how the relaxation time of uniaxial spins is affected by a weak field at an arbitrary direction, since it will allow us to study how the superparamagnetic blocking is affected by a field. This field dependence of the relaxation time can be obtained by expanding the relaxation rate $\Gamma = 1/\tau$ in powers of the field components. As the spins have inversion symmetry in the absence of a field, Γ should be an even function of the field components, and to third order it is given by

$$\Gamma \simeq \Gamma_0\Big(1 + c_{\parallel}\xi_{\parallel}^2 + c_{\perp}\xi_{\perp}^2\Big)\,, \tag{4.55}$$

where $\xi_{\parallel}$ and $\xi_{\perp}$ are the longitudinal and transversal components of the field (given in temperature units Eq. (4.8)) with respect to the anisotropy axis. Γ_0 is the zero-field relaxation rate, which for low temperatures ($\sigma > 1$) is given by Brown's result [95]

$$\Gamma_0 = \frac{1}{\tau_{\mathrm{D}}}\frac{2}{\sqrt{\pi}}\sigma^{3/2}e^{-\sigma}\,, \tag{4.56}$$

where $\tau_{\mathrm{D}} = m/(2\gamma\lambda k_{\mathrm{B}}T)$ is the relaxation time of isotropic spins. The coefficient $c_{\parallel}$ can be obtained by expanding the expression for Γ in the presence of a longitudinal field [95, 124]

$$\begin{aligned}\Gamma(\xi_{\parallel}, \xi_{\perp} = 0) &= \frac{1}{\tau_{\mathrm{D}}}\frac{\sigma^{3/2}}{\sqrt{\pi}}[(1+h)e^{-\sigma(1+h)^2} + (1-h)e^{-\sigma(1-h)^2}] \\ &\simeq \Gamma_0\Big(1 + \tfrac{1}{2}\xi_{\parallel}^2\Big)\,. \end{aligned} \tag{4.57}$$

There is no general expression for the relaxation rate in the presence of a non-zero transversal field valid for all values of the relevant parameters [125], but Garanin *et al.* have derived a low-temperature formula valid for weak transversal fields [111], which can be used to determine the coefficient $c_{\perp}$,

$$\Gamma(\xi_{\parallel} = 0, \xi_{\perp}) \simeq \Gamma_0\Big[1 + \tfrac{1}{4}F(\alpha)\xi_{\perp}^2\Big]\,, \tag{4.58}$$

$$F(\alpha) = 1 + 2(2\alpha^2 e)^{1/(2\alpha^2)}\gamma\left(1 + \frac{1}{2\alpha^2}\,,\, \frac{1}{2\alpha^2}\right)\,. \tag{4.59}$$

Here $\alpha = \lambda\,\sigma^{1/2}$ and $\gamma(a,z) = \int_0^z dt\, t^{a-1}\, e^{-t}$ is the incomplete gamma function. It can be noted that for the axially symmetric potential with a longitudinal field, the only dependence on λ is the trivial one in τ_{D}, while in the non-axially symmetric potential obtained with a transversal field the relaxation rate will strongly depend on λ through $F(\alpha)$ which is plotted in Fig. 4.5.

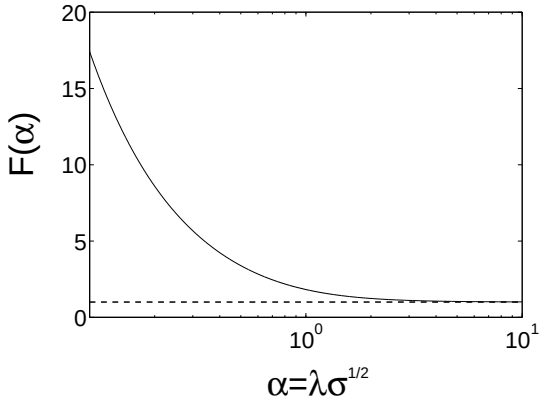

Figure 4.5: F vs $\alpha = \lambda\sigma^{1/2}$ (solid line) and the overdamped value $F = \frac{1}{4}$ (dashed line).

Collecting these results, we can finally write the expression for the relaxation rate in a weak field, obtained in Paper IX,

$$\Gamma \simeq \Gamma_0 \Big[1 + \tfrac{1}{2}\xi_{\parallel}^2 + \tfrac{1}{4} F(\alpha) \xi_{\perp}^2 \Big] \, . \tag{4.60}$$

4.4.3 Relaxation time of weakly interacting nanoparticles

The relaxation time for weakly interacting nanoparticles with uniaxial anisotropy can be obtained by inserting the thermodynamical averages of the dipolar fields (calculated in section 4.3.2) in the expression for the relaxation rate in a weak field Eq. (4.60). Earlier models [115, 116] have been energy-barrier based and therefore lack the dependence on λ. For instance, the model by Mørup and co-workers [116] is basically the same as the one presented here in the particular case of high damping and random anisotropy. The model by Mørup predicted a decrease of the blocking temperature with increasing interaction strength for weak interaction as was observed in high frequency Mössbauer experiments, while the Dormann-Bessias-Fiorani model [115] predicted an increase of the blocking temperature with increasing interaction strength as commonly observed in magnetisation measurements. These discrepancies led to some controversy [126, 127]. In Ref. [91] it was shown that for strong anisotropy (or weak interaction) the blocking temperature decreases with interaction (see Fig. 4.4), while for weak anisotropy (or moderate-to-high interaction) the energy barriers are governed by to the interaction and hence grow with h_d. An increase of the apparent blocking temperature is clearly the case for the strongly interacting nanoparticle samples studied in Chapter 5 in which the relaxation time increases with h_d due to spin-spin correlations (see Fig. 5.3).

In order to determine the characteristics of the superparamagnetic blocking we use the equilibrium susceptibility $\chi_{\rm eq}$ calculated using thermodynamic perturbation theory Eq. (4.28) and the relaxation rate Γ obtained when the dipolar fields Eq. (4.40) and (4.41) are introduced in Eq. (4.60). Combining

these expressions in a Debye-type formula,

$$\chi = \chi_{\rm eq} \frac{\Gamma}{\Gamma + i\omega} \tag{4.61}$$

provides us with a simple model for the dynamic response. The dynamic susceptibility of a large spherical sample with parallel anisotropy axis and a simple cubic structure is shown in Fig. 4.6. In the overdamped case, the blocking temperature is not noticeably affected by the dipolar interaction while for low damping the blocking temperature decreases significantly as the interaction strength increases. These results are in agreement with the simulations by Berkov and Gorn [91] shown in Fig. 4.4.

An interpretation of the strong damping dependence found in the presence of a transverse field component was given in Ref. [114]: The transverse field creates a saddle point in the potential barrier. A thermally excited spin with high damping will "fall" directly back to the bottom of the potential well if the thermal excitation is not large enough for an overbarrier jump. On the other hand, a weakly damped spin in the same situation will precess ($\sim 1/\lambda$ times) about the anisotropy axis and therefore has an increased probability for overbarrier jumps, each time it passes close to the saddle point. In the case of non-interacting particles the transverse field component must come from either a nonlinear probing field [114] or a bias field [113], while the transverse field here naturally arises from the dipolar interaction.

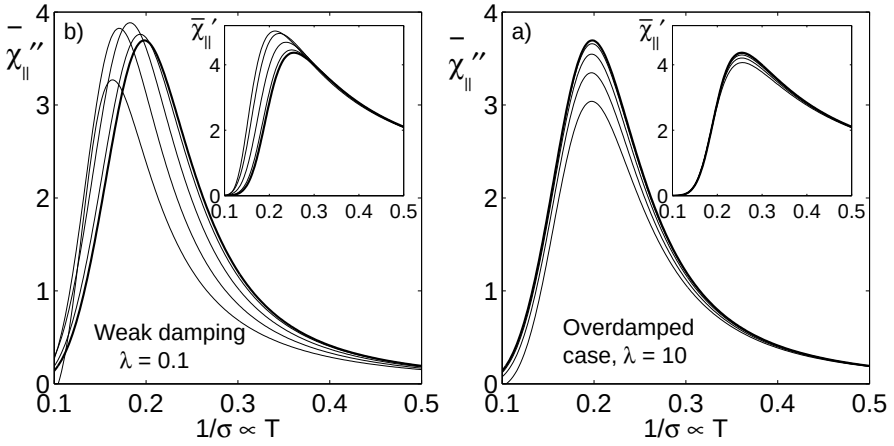

Figure 4.6: Imaginary component of the dynamical susceptibility vs temperature (the real component is shown in the inset) for a spherical sample and spins placed in a simple cubic lattice. The anisotropy axes are all parallel and the response is probed along their common direction. The dipolar interaction strength $h_{\rm d} = \xi_{\rm d}/2\sigma$ is: $h_{\rm d} = 0$ (thick lines), 0.004, 0.008, 0.012, and 0.016 from (a) right to left and (b) top to bottom. The frequency is $\omega\tau_{\rm D}/\sigma = 2\pi \times 0.003$.

4.5 Numerical methods

Due to the long-range and reduced symmetry of the dipole-dipole interaction analytical methods such as the thermodynamic perturbation theory presented in Sec. 4.3.2 will only be applicable for weak interaction. Numerical simulation techniques are therefore indispensable for the study of interacting nanoparticle systems, beyond the weak coupling regime.

The Monte Carlo (MC) method can be used to efficiently calculate thermal-equilibrium properties. However, since it is an energy-barrier based method it will fail to generate dynamic features such as the precession of the spins, and it is able to generate the dynamic magnetisation in the overdamped limit ($\lambda \to \infty$) only, if an appropriate algorithm is used [128].

Using a Langevin dynamics approach, the stochastic LLG equation (4.51) can be integrated numerically, in the context of the Stratonovich stochastic calculus, by choosing an appropriate numerical integration scheme [123]. This method was first applied to the dynamics of non-interacting particles [123] and later also to interacting particle systems [91].

Due to the long-range nature of the dipolar interaction, care must be taken in the evaluation of the dipolar field. For finite systems the sums in Eq. (4.12) are performed over all particles in the system. For systems with periodic boundary conditions the Ewald method [129, 130, 131], can be used to correctly calculate the conditionally convergent sum involved. However, in most work (e.g. [90, 91]) the simpler Lorentz-cavity method is used instead.

Chapter 5

Interacting nanoparticle systems

5.1 Introduction

There exist apparent resemblances between non-interacting nanoparticle systems and spin glasses as to the difference between the FC and ZFC magnetisation and the frequency dependent ac susceptibility. The origin of the slow dynamics in the two systems are different however, as discussed in the two previous chapters. It has been suggested that dense nanoparticle samples can exhibit glassy dynamics due to dipolar interparticle interaction [97]; disorder and frustration are induced by the randomness in the particle positions and anisotropy axes orientations. In order to investigate spin-glass-like properties of such systems, one needs to use the experimental techniques (protocols) developed in studies of spin glasses. Examining the effects of dipolar interactions using standard experimental protocols (ZFC/FC magnetisation or ac susceptibility) indicate no dramatic change in these quantities (c.f. Fig. 5.2) and one can be misled to believe that the only effect of the dipolar interaction is to increase the blocking temperature due to enhanced energy barriers. Some work, however, support the existence of glassy behaviour in such systems (e.g. [132, 133, 134]) and for strongly interacting systems with narrow size distributions evidence has been given for spin-glass-like phase transitions [135, 136, 137].

To know how the glassy behaviour affects various physical properties is not only of interest for the large number of applications using densely packed magnetic nanoparticles, but also from a fundamental point of view. Interacting nanoparticle systems are interesting as model systems for spin-glass-like dynamics. Due to a larger microscopic flip time in these systems, than in canonical spin glasses (see below), the time scales investigated in experiments are closer to those accessible by numerical simulation techniques [138].

5.2 Materials

Frozen ferrofluids offer systems where the dipolar interaction between the single-domain nanoparticles can be continuously varied by changing the particle concentration, and for all experiments on nanoparticles it is desirable to have a system with a narrow size distribution. The material that has been used in this study is a ferrofluid of single-domain particles of the amorphous alloy $Fe_{1-x}C_x$ ($x \approx 0.2$-0.3). The particle shape is nearly spherical (see Fig 5.1) and the average particle diameter $d = 5.3 \pm 0.3$ nm. The saturation magnetisation was estimated to $M_s = 1 \times 10^6$ Am^{-1}, the microscopic flip time to $\tau_0 = 1 \times 10^{-12}$ s, and the uniaxial anisotropy constant $K = 0.9 \times 10^5$ Jm^{-3}. For details on sample preparation and characterisation see Paper XII. This batch of $Fe_{1-x}C_x$ particles is slightly different from that studied in Refs. [135, 136]. We have studied samples with volume concentrations of $c = 17 \pm 4$, 5 ± 1, 1 ± 0.3 and 0.06 ± 0.02 vol% nanoparticles. The strength of the interaction for a given concentration is determined by the anisotropy constant and the saturation magnetisation according to Eq. (4.17) and for this sample $h_d \approx 0.56(c/100)$.

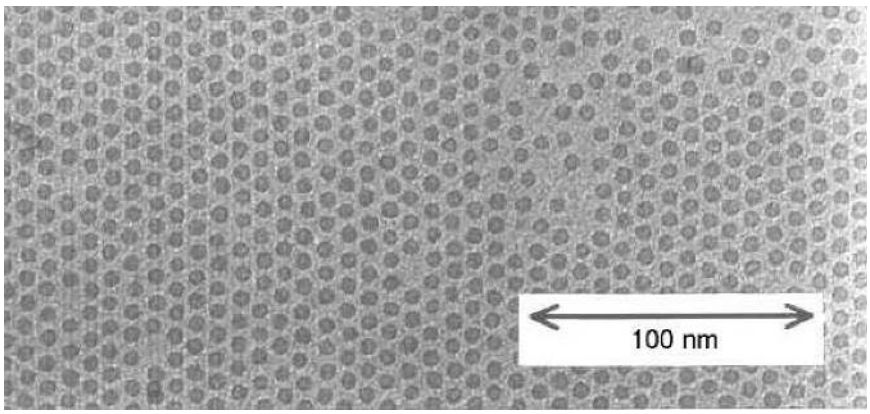

Figure 5.1: TEM picture of typical $Fe_{1-x}C_x$ nanoparticles.

5.3 A Spin-glass phase transition?

The existence of a second order phase transition can be evidenced from critical slowing down [Eq. (3.4)] approaching the phase transition from above. Defining a criterion for the onset of dissipation, we can extract the freezing temperature T_f associated with a certain relaxation time and derive the "transition" line (τ_c) between thermodynamic equilibrium and critical dynamics as in Fig. 3.2. Figure 5.2 shows the ac susceptibility for the 0.06, 5 and 17 vol% samples measured at two different frequencies. Data for a larger set of frequencies (shown in Paper XII) was used to extract the relaxation time versus T_f data for the 5 vol% sample and the 17 vol% sample shown in Fig. 5.3. The blocking temperature for the 0.06 vol% is shown in the same figure as a reference.

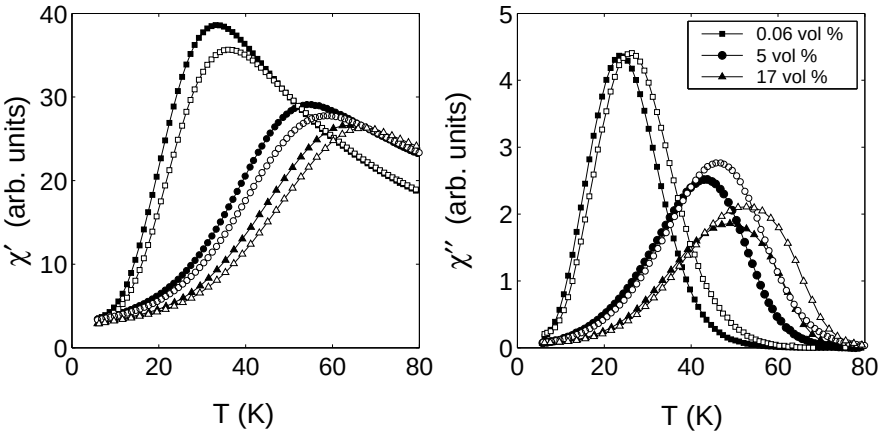

Figure 5.2: Ac susceptibility vs temperature at frequencies $\omega/2\pi = 125$ Hz (filled symbols) and $\omega/2\pi = 1000$ Hz (open symbols).

The dynamic susceptibility of a spin glass scales according to [139]

$$\frac{\chi''(T,\omega)}{\chi_{\rm eq}(T)} = \epsilon^{\beta} G(\omega\tau_c), \qquad T > T_{\rm g} \tag{5.1}$$

where $\omega = 1/t$ and $G(x)$ is a scaling function. It is shown in Fig. 5.4 that the susceptibility data for the 17 vol% sample could be scaled according to this relation and the parameters associated with the phase transition are indicated in the figure; from Paper XI. For the 5 vol% sample, the dynamic susceptibility

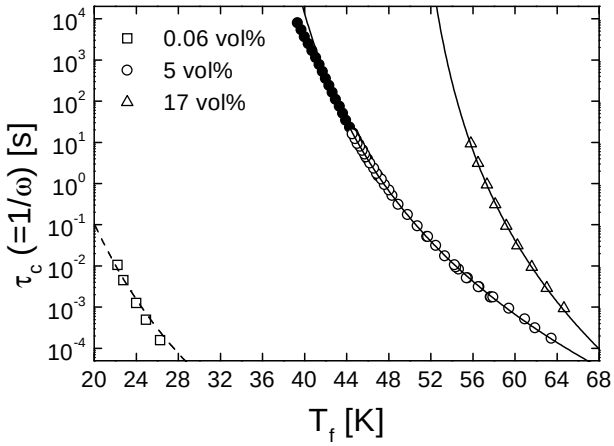

Figure 5.3: Relaxation time $\tau_c = \omega^{-1}$ vs $T_{\rm f}$. For the 5 vol% and 17 vol% samples the lines are fits to the critical slowing down relation [Eq. (3.4)] and for the 0.06 vol% sample a fit to the superparamagnetic relaxation time on the Arrhenius form Eq. (4.6).

could not be scaled according to Eq. (5.1).

For nanoparticles, τ_m in Eq. (3.4) can be assigned to the superparamagnetic relaxation time of a single particle. In Paper XII, we therefore included the exponential temperature dependence of τ_m in the analysis. This, however, only gives corrections to scaling and the exponents do not change significantly. Due to the temperature dependence of τ_m, a static scaling analysis as performed in Ref. [136] is a crucial additional tool to disclose a possible spin-glass phase transition in interacting nanoparticle systems.

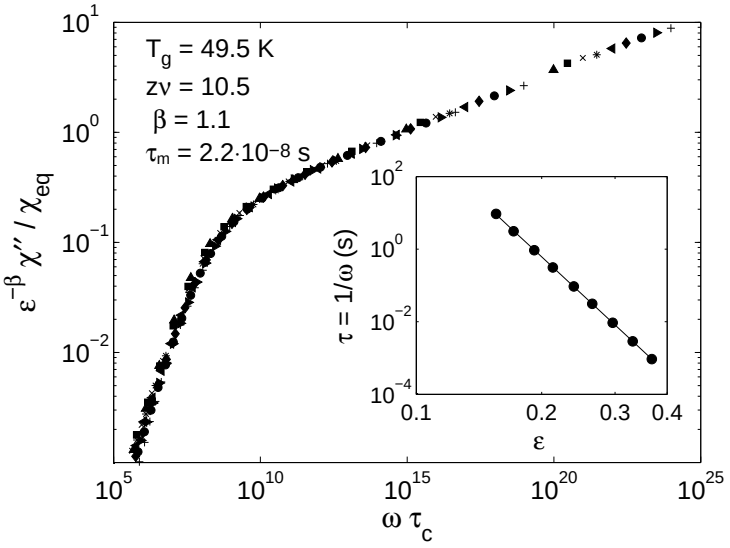

Figure 5.4: Scaling of $\epsilon^{-\beta}\chi''(T,\omega)/\chi_{\rm eq}$ data for $T > T_{\rm g}$ for the 17 vol% sample. Inset: critical slowing down analysis on a log-log scale.

5.4 Glassy dynamics

The ZFC relaxation for a noninteracting nanoparticle sample is only a function of the relaxation time and the volume distribution of particles in the sample. Magnetic ageing, as shown in Fig. 5.5 for the 5 vol% sample, is therefore a clear evidence for glassy dynamics. In Paper X, we have examined the glassy dynamics of the 5 vol% sample using the ac memory method presented in Sec. 3.4. As for the $Fe_{0.50}Mn_{0.50}TiO_3$ sample, the ac susceptibility measured on heating is lower than the one measured on cooling. A double stop memory experiment is shown in Fig. 5.6 together with the two corresponding single stop experiments. In this figure χ' is shown instead of χ'' since the relaxation is larger in χ', and the nonequilibrium effects are more clearly revealed by subtracting the reference curves obtained on constant cooling (respectively heating). This sample exhibits qualitatively similar ageing, memory and rejuvenation phenomena, as the spin glasses studied in chapter 3. The rejuvenation effect is however much weaker; the cooling curve approaches the reference curve only very slowly and

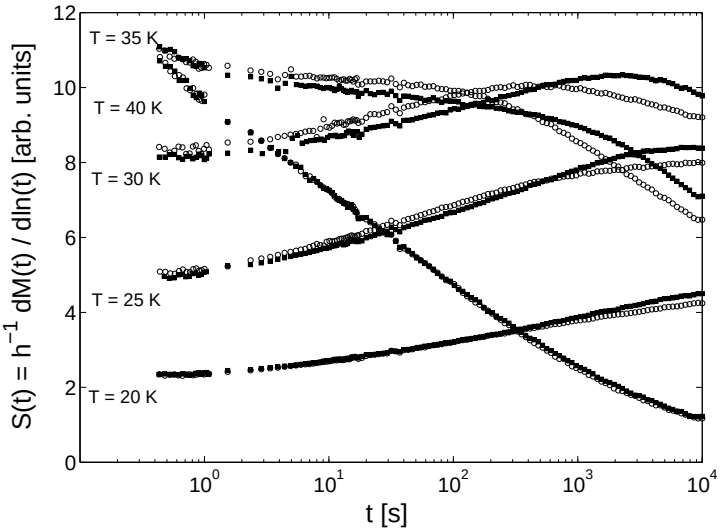

Figure 5.5: $S(t)$ vs time on a logarithmic scale for the 5 vol% sample obtained from ZFC relaxation measurements with $t_{\rm w} = 300$ s (open symbols) and 3000 s (filled symbols).

if the two stops are made somewhat closer in temperature as in Fig. 5.7, the heating curve only exhibit one dip.

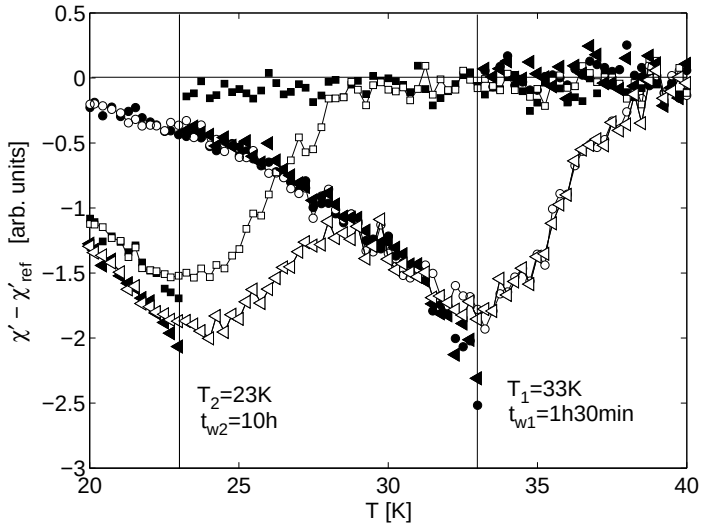

Figure 5.6: $\chi'(T) - \chi'_{\rm ref}(T)$ vs T measured on cooling (solid symbols) and heating (open symbols) for the 5 vol% sample. Circles, the cooling was halted at 33 K for 1 h 30 min; squares, the cooling was halted at 23 K for 10h and triangles, the cooling was halted at $T_1 = 33$ K for $t_{\rm w_1} = 1$ h 30 min and at $T_2 = 23$ K for $t_{\rm w_2} = 10$ h. $\omega/2\pi = 510$ mHz.

This nanoparticle sample can, due to the uniaxial anisotropy of the individual particles and the anisotropic interparticle interaction, be considered as an Ising spin glass. The relative time scales ($t_{\rm obs}/\tau_m$) of the experiments on nanoparticle systems are shorter than for conventional spin glasses, due to the larger microscopic flip time. The nonequilibrium phenomena observed here are indeed rather similar to those observed in numerical simulations on the Ising EA model [138], which also correspond to shorter time (length) scales [39]. It would be interesting to examine if the nonequilibrium phenomena are different in a more dense sample with stronger interparticle interactions. Due to some technical difficulties such a study was unfortunately not possible to perform on the 17 vol% sample.

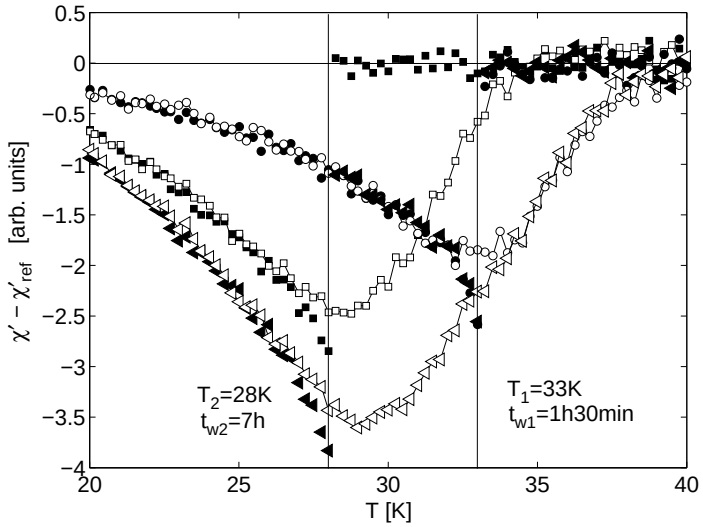

Figure 5.7: $\chi'(T) - \chi'_{\rm ref}(T)$ vs T measured on cooling (solid symbols) or heating (open symbols) for the 5 vol% sample. Circles, the cooling was halted at 33 K for 1 h 30 min; squares, the cooling was halted at 28 K for 7 h and triangles, the cooling was halted at $T_1 = 33$ K for $t_{\rm w_1} = 1$ h 30 min and at $T_2 = 28$ K for $t_{\rm w_1} = 7$ h. $\omega/2\pi = 510$ mHz.

5.5 Dynamics in a field

The ageing dynamics in a bias field was studied in Paper XIV. The ageing dynamics is found to be strongly affected by the bias field, in a qualitatively similar way to spin glass dynamics. It was shown that the ageing disappears completely in a strong enough field. Figure 5.8 shows the ac susceptibility in superimposed dc fields for the 5 and 1 vol% samples. It can be seen that for high enough fields, the susceptibility curves for the two samples are almost identical, showing that the effects of dipolar interaction are suppressed by a strong enough magnetic field.

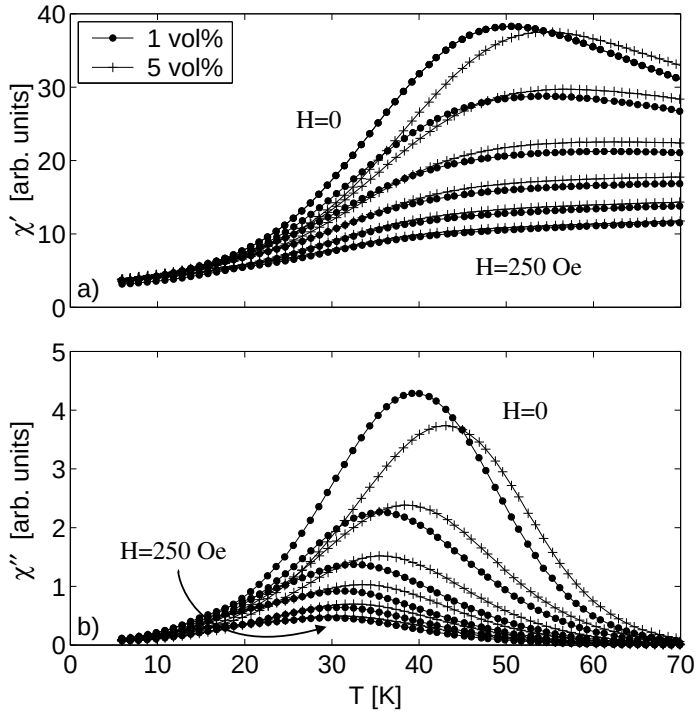

Figure 5.8: The ac susceptibility vs temperature for different superimposed dc fields; H = 0, 50, 100, 150, 200, 250 Oe. $\omega/2\pi = 125$ Hz.

Appendix: S_l for uniaxial anisotropy

The thermodynamical average $S_l(\sigma)$ over the Legendre polynomials P_l occur in the expressions for the susceptibilities, the specific heat and the dipolar fields in Sec. 4.3. For uniaxial anisotropy these averages read

$$S_l(\sigma) = \langle P_l \rangle_a = \frac{1}{\mathcal{Z}_a} \int_{-1}^{1} dz P_l(z) e^{\sigma z^2} \,. \tag{5.2}$$

In particular, $S_0 = 1$ and $S_2 = \frac{1}{2} \left\langle 3z^2 - 1 \right\rangle_a$ [Eq. (4.21)] can be written,

$$S_2 = \frac{3}{2} \left(\frac{e^\sigma}{\sigma \mathcal{Z}_a} - \frac{1}{2\sigma} \right) - \frac{1}{2} \,. \tag{5.3}$$

The one-spin partition function $\mathcal{Z}_a = \int_{-1}^{1} dz \, \exp(\sigma z^2)$ can be written in terms of *error* functions of real and "imaginary" argument as

$$\mathcal{Z}_a = \begin{cases} \sqrt{\pi/\sigma}\, \mathrm{erfi}(\sqrt{\sigma}), & \sigma > 0 \\ \sqrt{\pi/|\sigma|}\, \mathrm{erf}(\sqrt{|\sigma|}), & \sigma < 0 \end{cases} \tag{5.4}$$

The less familiar $\mathrm{erfi}(x)$ is related with the Dawson integral $D(x)$, so in the easy-axis case one can write $Z_\mathrm{a} = (2e^\sigma/\sqrt{\sigma}) D(\sqrt{\sigma})$ and compute $D(x)$ with the subroutine `DAWSON` of Ref. [140].

For $l > 2$ the S_l can be computed using the following homogeneous three-term recurrence relation [141]

$$\left[1 - \frac{2\sigma}{(2l-1)(2l+3)} \right] S_l - \frac{2\sigma}{2l+1} \left[\frac{l-1}{2l-1} S_{l-2} - \frac{l+2}{2l+3} S_{l+2} \right] = 0 \,, \tag{5.5}$$

The derivative of any S_l can be computed by means of the differential-recurrence relation derived in Paper VIII

$$\begin{aligned} S_l' = \frac{dS_l}{d\sigma} \quad = \quad & \frac{(l-1)l}{(2l-1)(2l+1)} S_{l-2} + \frac{2l(l+1)}{3(2l-1)(2l+3)} S_l \\ & + \frac{(l+1)(l+2)}{(2l+1)(2l+3)} S_{l+2} - \frac{2}{3} S_2 S_l \,. \end{aligned} \tag{5.6}$$

The approximate behaviour of S_2 for weak ($|\sigma| \ll 1$) and strong ($|\sigma| \gg 1$) anisotropy is

$$S_2(\sigma) = \begin{cases} \frac{2}{15}\sigma + \frac{4}{315}\sigma^2 + \cdots & |\sigma| \ll 1 \\ 1 - \frac{3}{2\sigma} - \frac{3}{4\sigma^2} + \cdots & \sigma \gg 1 \\ -\frac{1}{2}(1 + \frac{3}{2\sigma}) + \cdots & \sigma \ll -1 \end{cases} . \quad (5.7)$$

Bibliography

[1] V. Cannella and J. A. Mydosh, Phys. Rev. B **6**, 4220 (1972).

[2] E. C. Stoner and E. P. Wohlfart, Philos. Trans. R. Soc. London Ser. A **240**, 599 (1948).

[3] L. Néel, Ann. Geophys. **5**, 99 (1949).

[4] W. Heisenberg, Z. Phys. **49**, 619 (1928).

[5] E. Ising, Z. Phys. **31**, 253 (1925).

[6] S. F. Edwards and P. W. Anderson, J. Phys. F **5**, 965 (1975).

[7] D. Sherrington and S. Kirkpartick, Phys. Rev. Lett. **35**, 1792 (1975).

[8] G. Toulouse, Comm. Phys. **2**, 115 (1977).

[9] J. M. Yeomans, *Statistical Mechanics of Phase Transitions* (Oxford University Press, Oxford, 1992).

[10] S. K. Ma, *Modern Theory of Critical Phenomena* (Addison-Wesley Publishing, New York, 1976).

[11] K. G. Wilson, Phys. Rev. B **4**, 3174 (1971).

[12] K. G. Wilson, Phys. Rev. B **4**, 3184 (1971).

[13] J. Magnusson, C. Djurberg, P. Granberg, and P. Nordblad, Rev. Sci. Instrum. **68**, 3761 (1997).

[14] K. Binder and A. P. Young, Rev. Mod. Phys. **58**, 801 (1986).

[15] H. Aruga, T. Tokoro, and A. Ito, J. Phys. Soc. Jpn. **57**, 261 (1988).

[16] K. Gunnarsson, P. Svedlindh, P. Nordblad, L. Lundgren, H. Aruga, and A. Ito, Phys. Rev. Lett. **61**, 754 (1988).

[17] K. Gunnarsson, P. Svedlindh, P. Nordblad, L. Lundgren, H. Aruga, and A. Ito, Phys. Rev. B **43**, 8199 (1991).

[18] R. N. Bhatt and A. P. Young, Phys. Rev. B **37**, 5606 (1988).

[19] N. Kawashima and A. P. Young, Phys. Rev. B **53**, R484 (1996).

[20] H. G. Ballestros, A. Cruz, L. A. Fernandez, V. Martin-Mayor, J. Pech, J. J. Ruiz-Lorenzo, A. Tarancon, and P. Tellez, Phys. Rev. B **62**, 14237 (2000).

[21] L. P. Lévy, Phys. Rev. B **38**, 4963 (1988).

[22] B. Leclercq, C. Rigaux, A. Mycielski, and M. Menant, Phys. Rev. B **47**, 6169 (1993).

[23] J. A. Olive, A. P. Young, and D. Sherrington, Phys. Rev. B **34**, 6341 (1986).

[24] H. Kawamura, Phys. Rev. Lett. **68**, 3785 (1992).

[25] H. Kawamura, Phys. Rev. Lett. **80**, 5421 (1998).

[26] K. Hukushima and H. Kawamura, Phys. Rev. E **61**, R1008 (2000).

[27] R. W. Walstedt and L. R. Walker, Phys. Rev. Lett. **47**, 1624 (1981).

[28] F. Matsuba, T. Iyota, and S. Inawashiro, Phys. Rev. Lett. **67**, 1458 (1991).

[29] D. Petit, L. Fruchter, and I. A. Campbell, cond-mat/0111129, to appear in Phys. Rev. Lett..

[30] L. C. A. Struik, *Physical aging in amorphous polymers and other materials* (Elsevier, Amsterdam, 1978).

[31] J. Hammann, E. Vincent, V. Dupuis, M. Alba, M. Ocio, and J.-P. Bouchaud, J. Phys. Soc. Jpn. **69** Suppl. A, 226 (2000).

[32] L. Bellon, S. Ciliberto, and C. Laroche, Europhys. Lett. **51**, 551 (2000).

[33] P. Doussineau, T. de Lacerda-Arôso, and A. Levelut, Europhys. Lett. **46**, 401 (1999).

[34] V. Normand, S. Muller, J.-C. Ravey, and A. Parker, Macromolecules **33**, 1063 (2000).

[35] E. L. Papadopoulou, P. Nordblad, P. Svedlindh, R. Schöneberger, and R. Gross, Phys. Rev. Lett. **82**, 173 (1999).

[36] K. Jonason, E. Vincent, J. Hammann, J.-P. Bouchaud, and P. Nordblad, Phys. Rev. Lett. **81**, 3243 (1998).

[37] H. Yoshino, A. Lemaître, and J.-P. Bouchaud, Eur. Phys. J. B **20**, 367 (2001).

[38] J.-P. Bouchaud, V. Dupuis, J. Hammann, and E. Vincent, Phys. Rev. B **65**, 024439 (2001).

[39] L. Berthier and J. P. Bouchaud, cond-mat/0202069.

[40] M. Sales and H. Yoshino, cond-mat/0112384 and cond-mat/0203371.

[41] F. Krzakala and O. C. Martin, cond-mat/0203449.

[42] M. A. Ruderman and C. Kittel, Phys. Rev. **96**, 99 (1954).

[43] T. Kasuya, Prog. Theor. Phys. **16**, 45 and 58 (1956).

[44] K. Yosida, Phys. Rev. **106**, 893 (1957).

[45] A. Fert and P. M. Levy, Phys. Rev. Lett. **44**, 1538 (1980).

[46] J. J. Prejean, M. J. Joliclerc, and P. Monod, J. Physique **41**, 427 (1980).

[47] A. Ito, H. Aruga, E. Torikai, M. Kikuchi, Y. Syono, and H. Takei, Phys. Rev. Lett. **57**, 483 (1986).

[48] A. Ito, E. Torikai, S. Morimoto, H. Aruga, M. Kikuchi, Y. Syono, and H. Takei, J. Phys. Soc. Jpn. **59**, 829 (1990).

[49] H. Aruga Katori and A. Ito, J. Phys. Soc. Jpn. **62**, 4488 (1993).

[50] A. Seidel, K. Gunnarsson, L. Häggström, P. Svedlindh, H. Aruga Katori, and A. Ito, J. Phys.: Condens. Matter **5**, 615 (1993).

[51] W. L. McMillan, J. Phys. C **17**, 3179 (1984).

[52] A. J. Bray and M. A. Moore, in *Heidelberg Colloquium on Glassy Dynamics*, edited by J. L. van Hemmen and I. Morgenstern (Springer, Berlin, 1986).

[53] D. S. Fisher and D. A. Huse, Phys. Rev. Lett. **56**, 1601 (1986).

[54] D. S. Fisher and D. A. Huse, Phys. Rev. B **38**, 386 (1988).

[55] D. S. Fisher and D. A. Huse, Phys. Rev. B **38**, 373 (1988).

[56] G. Parisi, Phys. Rev. Lett. **43**, 1754 (1979).

[57] G. Parisi, J. Phys. A **13**, 1101 (1980).

[58] G. Parisi, Phys. Rev. Lett. **50**, 1946 (1983).

[59] H. Yoshino, K. Hukushima, and H. Takayama, cond-mat/0203267.

[60] M. Palassini and A. P. Young, Phys. Rev. Lett. **85**, 3017 (2000).

[61] A. J. Bray and M. A. Moore, J. Phys. C **17**, L463 (1984).

[62] A. K. Hartmann and A. P. Young, Phys. Rev. B **64**, 180404 (2001).

[63] A. C. Carter, A. J. Bray, and M. A. Moore, Phys. Rev. Lett. **88**, 077201 (2002).

[64] A. K. Hartmann, Phys. Rev. E **59**, 84 (1999).

[65] T. Komori, H. Yoshino, and H. Takayama, J. Phys. Soc. Jpn. **69**, 1192 (2000).

[66] H. Risken, *The Fokker–Planck Equation*, 2nd ed. (Springer, Berlin, 1989).

[67] A. G. Schins, A. F. M. Arts, and H. W. Wijn, Phys. Rev. Lett. **70**, 2340 (1993).

[68] K. Hukushima, H. Yoshino, and H. Takayama, Prog. Theo. Phys. **138**, 568 (2000).

[69] J. Kisker, L. Santen, M. Schrenckenberg, and H. Rieger, Phys. Rev. B **53**, 6418 (1996).

[70] E. Marinari, G. Parisi, F. Ricci-Tersenghi, and J. J. Ruiz-Lorenzo, J. Phys. A **31**, 2611 (1998).

[71] T. Komori, H. Yoshino, and H. Takayama, J. Phys. Soc. Jpn. **68**, 3387 (1999).

[72] A. J. Bray and M. A. Moore, Phys. Rev. Lett. **58**, 57 (1987).

[73] J. Mattsson, T. Jonsson, P. Nordblad, H. Aruga Katori, and A. Ito, Phys. Rev. Lett. **74**, 4305 (1995).

[74] J. R. L. d'Almeida and D. J. Thouless, J. Phys. A **11**, 983 (1978).

[75] M. Gabay and G. Toulouse, Phys. Rev. Lett. **47**, 201 (1981).

[76] H. Kawamura and D. Imagawa, Phys. Rev. Lett. **87**, 207203 (2001).

[77] D. Petit, L. Fruchter, and I. A. Campbell, Phys. Rev. Lett. **83**, 5130 (1999).

[78] L. Lundgren, P. Svedlindh, P. Nordblad, and O. Beckman, Phys. Rev. Lett. **51**, 911 (1983).

[79] P. Granberg, L. Sandlund, P. Nordblad, P. Svedlindh, and L. Lundgren, Phys. Rev. B **38**, 7079 (1988).

[80] J. O. Andersson, J. Mattsson, and P. Nordblad, Phys. Rev. B **48**, 13977 (1993).

[81] J.-P. Bouchaud and D. Dean, J. Phys. I **5**, 265 (1995).

[82] J. Houdayer and O. C. Martin, Europhys. Lett. **49**, 794 (2000).

[83] F. Krzakala and O. C. Martin, Phys. Rev. Lett. **85**, 3013 (2000).

[84] E. Vincent, J. Hammann, M. Ocio, J.-P. Bouchaud, and L. F. Cugliandolo, in *Complex behaviour of glassy systems: proceedings of the XIV Sitges Conference*, edited by E. Rubi (Springer, Berlin, 1996).

[85] V. Dupuis, E. Vincent, J.-P. Bouchaud, J. Hammann, A. Ito, and H. Aruga Katori, Phys. Rev. B **64**, 174204 (2001).

[86] F. Matsubara, S. Endoh, and T. Shirakura, J. Phys. Soc. Jpn. **69**, 1927 (2000).

[87] W. Wernsdorfer, E. Bonet Orozco, K. Hasselbach, A. Benoit, B. Barbara, N. Demoncy, A. Loiseau, H. Pascard, and D. Mailly, Phys. Rev. Lett. **78**, 1791 (1997).

[88] M. A. Załuska-Kotur and M. Cieplak, Europhys. Lett. **23**, 85 (1993).

[89] M. A. Załuska-Kotur, Phys. Rev. B **54**, 1064 (1996).

[90] J.-O. Andersson, C. Djurberg, T. Jonsson, P. Svedlindh, and P. Nordblad, Phys. Rev. B **56**, 13 983 (1997).

[91] D. V. Berkov and N. L. Gorn, J. Phys.: Condens. Matter **13**, 9369 (2001).

[92] S. Chikazumi, *Physics of Ferromagnetism*, 2nd ed. (Oxford University Press, Oxford, 1997).

[93] F. Gazeau, J. C. Bacri, F. Gendron, R. Perzynski, Y. L. Raĭkher, V. I. Stepanov, and E. Dubois, J. Magn. Magn. Mater. **186**, 175 (1998).

[94] R. V. Upadhyay, D. Srinivas, and R. V. Mehta, J. Magn. Magn. Mater. **214**, 105 (2000).

[95] W. F. Brown, Jr., Phys. Rev. **130**, 1677 (1963).

[96] C. P. Bean and J. D. Livingston, J. Appl. Phys. **30**, 120s (1959).

[97] W. Luo, S. R. Nagel, T. F. Rosenbaum, and R. E. Rosensweig, Phys. Rev. Lett. **67**, 2721 (1991).

[98] J. L. García-Palacios, Adv. Chem. Phys. **112**, 1 (2000).

[99] J. L. García-Palacios and F. J. Lázaro, Phys. Rev. B **55**, 1006 (1997).

[100] Y. L. Raĭkher and V. I. Stepanov, Phys. Rev. B **55**, 15 005 (1997).

[101] R. Pierls, Z. Phys. **80**, 763 (1933).

[102] L. D. Landau and E. M. Lifshitz, *Statistical Physics*, 2nd ed. (Pergamon Press, Oxford, 1970).

[103] B. Huke and M. Lücke, Phys. Rev. E **62**, 6875 (2000).

[104] I. Waller, Z. Phys. **104**, 132 (1936).

[105] J. H. van Vleck, J. Chem. Phys. **5**, 320 (1937).

[106] R. B. Griffiths, Phys. Rev. **176**, 655 (1968).

[107] S. Banerjee, R. B. Griffiths, and M. Widom, J. Stat. Phys. **93**, 109 (1998).

[108] J. A. Pople, Phil. Mag. **44**, 1276 (1953).

[109] W. T. Coffey, D. S. F. Crothers, J. L. Dormann, L. J. Geoghegan, and E. C. Kennedy, Phys. Rev. B **58**, 3249 (1998).

[110] W. T. Coffey, D. S. F. Crothers, J. L. Dormann, L. J. Geoghegan, E. C. Kennedy, and W. Wernsdorfer, J. Phys.: Condens. Matter **10**, 9093 (1998).

[111] D. A. Garanin, E. C. Kennedy, D. S. F. Crothers, and W. T. Coffey, Phys. Rev. E **60**, 6499 (1999).

[112] W. T. Coffey, D. S. F. Crothers, J. L. Dormann, Y. P. Kalmykov, E. C. Kennedy, and W. Wernsdorfer, Phys. Rev. Lett. **80**, 5655 (1998).

[113] W. T. Coffey, D. S. F. Crothers, Y. P. Kalmykov, and S. V. Titov, Phys. Rev. B **64**, 012411 (2001).

[114] J. L. García-Palacios and P. Svedlindh, Phys. Rev. Lett. **85**, 3724 (2000).

[115] J. L. Dormann, L. Bessais, and D. Fiorani, J. Phys. C **21**, 2015 (1988).

[116] S. Mørup and E. Tronc, Phys. Rev. Lett. **72**, 3278 (1994).

[117] R. Kubo and N. Hashitsume, Prog. Theor. Phys. **46**, 210 (1970).

[118] W. T. Coffey, P. J. Cregg, and Y. P. Kalmykov, Adv. Chem. Phys. **83**, 263 (1993).

[119] T. L. Gilbert, Phys. Rev. **100**, 1243 (1955).

[120] L. D. Landau and E. M. Lifshitz, Z. Phys. Sowjet. **8**, 153 (1935).

[121] Y. L. Raĭkher and V. I. Stepanov, Phys. Rev. B **50**, 6250 (1994).

[122] R. Kubo, Rep. Prog. Phys. **29**, 255 (1966).

[123] J. L. García-Palacios and F. J. Lázaro, Phys. Rev. B **58**, 14 937 (1998).

[124] A. Aharoni, Phys. Rev. **177**, 793 (1969).

[125] W. T. Coffey, D. A. Garanin, H. Kachkachi, and D. J. McCarthy, J. Magn. Magn. Mater. **221**, 110 (2000).

[126] M. F. Hansen and S. Mørup, J. Magn. Magn. Mater. **184**, 262 (1998).

[127] J. L. Dormann, D. Fiorani, and E. Tronc, J. Magn. Magn. Mater. **202**, 251 (1999).

[128] U. Nowak, R. W. Chantrell, and E. C. Kennedy, Phys. Rev. Lett. **84**, 163 (2000).

[129] P. Ewald, Ann. Phys. **64**, 253 (1921).

[130] E. Madelung, Phys. Z. **19**, 524 (1918).

[131] S. W. de Leeuw, J. W. Perram, and E. R. Smith, Proc. R. Soc. Lond. A **373**, 27 (1980).

[132] T. Jonsson, J. Mattsson, C. Djurberg, F. A. Khan, P. Nordblad, and P. Svedlindh, Phys. Rev. Lett. **75**, 4138 (1995).

[133] H. Mamiya, I. Nakatani, and T. Furubayashi, Phys. Rev. Lett. **82**, 4332 (1999).

[134] J. L. Dormann, D. Fiorani, R. Cherkaoui, E. Tronc, F. Lucari, F. D'Orazio, L. Spinu, M. Noguès, H. Kachkachi, and J. P. Jolivet, J. Magn. Magn. Mater. **203**, 23 (1999).

[135] C. Djurberg, P. Svedlindh, P. Nordblad, M. F. Hansen, F. Bødker, and S. Mørup, Phys. Rev. Lett. **79**, 5154 (1997).

[136] T. Jonsson, P. Svedlindh, and M. F. Hansen, Phys. Rev. Lett. **81**, 3976 (1998).

[137] S. Sahoo, O. Petracic, C. Binek, W. Kleemann, J. B. Sousa, S. Cardoso, and P. P. Freitas, Phys. Rev. B **65**, 134406 (2002).

[138] T. Komori, H. Yoshino, and H. Takayama, J. Phys. Soc. Jpn. **69** Suppl. A, 228 (2000).

[139] C. Rigaux, Ann. Phys. Fr. **20**, 445 (1995).

[140] W. H. Press, S. A. Teukolsky, W. T. Vetterling, and B. P. Flannery, *Numerical Recipes*, 2nd ed. (Cambridge University Press, New York, 1992).

[141] Y. P. Kalmykov and W. T. Coffey, Phys. Rev. B **56**, 3325 (1997).

Acknowledgements

First, I would like to thank my supervisor Per Nordblad and my co-supervisor José García-Palacios for their patience, encouragement and explanations. I also thank Peter Svedlindh and Professor Claes-Göran Granqvist for accepting me as a PhD student to the Solid State Physics group. The low-temperature experiments would not have been possible without the liquid helium and nitrogen: Thank you Erland!

I would like to thank Dr. Hajime Yoshino for collaboration, enthusiasm and many ideas. Dr. Mikkel Fougt Hansen is also gratefully acknowledged for collaboration and sample preparation.

Marie Vennström is thanked for her skillful help with sample preparation and Bengt Götesson for his technical assistance.

I would also like to thank Anna Andersson for sharing her apartment during my first time in Uppsala and for the later collaboration.

Economic travel support from Anna-Maria Lundins Stipendiefond for Roland Mathieu and myself is gratefully acknowledged. I would at the same time like to thank all our kind hosts in Japan: Dr. H. Yoshino, Prof. H. Kawamura, Dr. K. Hukushima, Prof. H. Takayama, Prof. A. Asamitsu and Prof. Y. Tokura. Prof. T. Sato is acknowledged for his time in Sweden and ours in Japan.

I would like to thank all present and past members of the Solid State Physics group and in particular those of the magnetism group: Olle, Per G, Tomas, Kristian, Arvid, Evie, Nam, Örjan, Solveig, Mehreteab, Salee and Victor.

Thank you Roland for your support, encouragements and ... everything!

This work has partially been financed by the Swedish Research Council.

Uppsala, April 25^{th} 2002

Petra Jönsson